

Institut für Angewandte Physik
der Universität Bonn

Wegelerstraße 8
53115 Bonn

Harmonic Generation with Optical Microfibres under Controlled Atmospheres

von
Sandro Fabian Bruse

Diplomarbeit in Physik

angefertigt im
Institut für Angewandte Physik

vorgelegt der
Mathematisch-Naturwissenschaftlichen Fakultät
der Rheinischen Friedrich-Wilhelms-Universität
Bonn
im Februar 2011

Referent: Prof. Dr. D. Meschede
Korreferent: Prof. Dr. M. Fiebig

Contents

| | | |
|----------|---|-----------|
| 1 | Introduction | 5 |
| 2 | Optical microfibres | 7 |
| 2.1 | Microfibres design | 7 |
| 2.2 | Microfibre manufacturing | 9 |
| 2.3 | Microfibre properties | 10 |
| 2.3.1 | Light propagation in OMF | 10 |
| 2.3.2 | Harmonic generation in OMF | 10 |
| 2.3.3 | Phase matching | 11 |
| 3 | Caesium | 13 |
| 3.1 | Nonlinearity of caesium | 13 |
| 3.1.1 | Wavelength dependence of $\chi^{(3)}$ | 13 |
| 3.1.2 | Vapour pressure | 14 |
| 3.2 | Light absorbed by caesium | 16 |
| 3.2.1 | Voigt profile | 16 |
| 3.2.2 | Hyperfine splitting | 17 |
| 4 | Experimental setup | 21 |
| 4.1 | Apparatus | 22 |
| 4.1.1 | Vacuum system | 22 |
| 4.1.2 | Heating system | 24 |
| 4.1.3 | Optical setup | 26 |
| 4.2 | Using fibre samples | 26 |
| 4.2.1 | Types of optical fibres | 26 |
| 4.2.2 | Fibre in the vacuum chamber | 27 |
| 4.3 | Caesium in the chamber | 29 |
| 4.4 | Challenges and limitations | 30 |
| 5 | Caesium detection | 33 |
| 5.1 | Absorption spectroscopy | 33 |
| 5.1.1 | Setup | 33 |
| 5.1.2 | Frequency calibration | 34 |
| 5.1.3 | Measured absorption | 35 |

| | | |
|----------|---|-----------|
| 5.1.4 | Influences on the dip shape | 37 |
| 5.2 | Effects of caesium vapour | 38 |
| 5.3 | Characterizing the caesium absorption dip | 38 |
| 5.3.1 | Absorption with different laser powers | 38 |
| 5.3.2 | Temporal evolution of the absorption | 39 |
| 5.3.3 | Cleaning the fibre with light | 40 |
| 6 | Third harmonic generation with caesium | 43 |
| 6.1 | Setup | 43 |
| 6.2 | Characterising THG without caesium | 44 |
| 6.3 | THG in caesium vapour | 45 |
| 6.4 | Discussion | 45 |
| 7 | Summary and outlook | 47 |
| A | Harmonic generation without caesium | 51 |
| A.1 | Third harmonic generation in air and vacuum | 51 |
| A.2 | THG in vacuum and dry nitrogen | 51 |
| A.3 | SHG in air, vacuum and dry nitrogen | 52 |
| A.4 | OMF transmission in air and vacuum | 54 |
| A.5 | Results and discussion | 56 |

Chapter 1

Introduction

Fibre optics is currently a rapidly developing field in physics. Fibres are more than just a waveguide, today they take the technical progress in telecommunication and medicine to the next level. But they are also a state of the art tool for fundamental physics.

In particular optical waveguides with submicrometre diameters have been of interest during the last years due to a whole range of unique properties. In such a microfibre, light is tightly confined over a large length of up to several centimetres. This high intensity “infinite focus” is accessible from outside the fibre due to the strong evanescent field. It makes optical microfibres an useful tool for light-matter interaction experiments.

To explore the applicability of OMF for nonlinear spectroscopy, I studied the interaction of gaseous caesium with the evanescent light field of the microfibre. For this purpose, the microfibre has been placed into a caesium vapour in a heated vacuum chamber.

In the first part of this work, the unambiguous optical detection of caesium is presented. This was done using a modified saturation spectroscopy method, where it was possible to detect caesium vapour by light absorption in the evanescent field of the fibre. In a next step the caesium vapour in the chamber has been characterised and its temporal evolution has been studied.

After detecting caesium, I have investigated the nonlinear light-matter interaction in the evanescent field of an optical microfibre. The high intensities around the microfibre were used to achieve harmonic generation in the presence and absence of a caesium vapour. The results provide an insight into the sensitivity of this effect and its dependence on the material around the fibre.

Finally I can conclude that optical microfibres can be used as sensitive detectors for atomic vapours, but also as a platform for nonlinear optics research.

Chapter 2

Optical microfibres

2.1 Microfibres design

Optical microfibres (OMF) are circular optical waveguides with a sub-micrometre diameter. They are produced from bare, standard (commercial) optical fibres. A typical optical fibre is shown in Fig. 2.1. It consists of a core and a cladding, as well as a coating for protection. The refractive index of the core is higher than the one of the cladding. Light coupled into the core is therefore guided due to total internal reflection at the core-cladding interface.

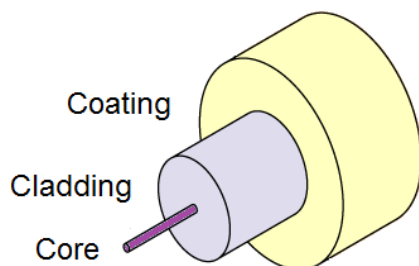


Figure 2.1: Standard optical fibre with core (violet), cladding (blue) and a coating (yellow).

An OMF is pulled from such a fibre using the so called flame-brushing process [1, 2]. The fibre coating is removed for this process. After pulling, our OMF samples consist of an unprocessed pigtail, a down-taper, a constant-diameter thin part (waist), an up-taper, and another pigtail (Fig. 2.2). The waist diameter is on the order of 300 nm to 500 nm.

In the waist the refractive index step between the cladding and air (or vacuum) is large. This and the small diameter of the waist cause a strong transverse confinement of the propagating mode and a strong evanescent field. More than half of the total power is guided around the fibre waist (Fig. 2.2).

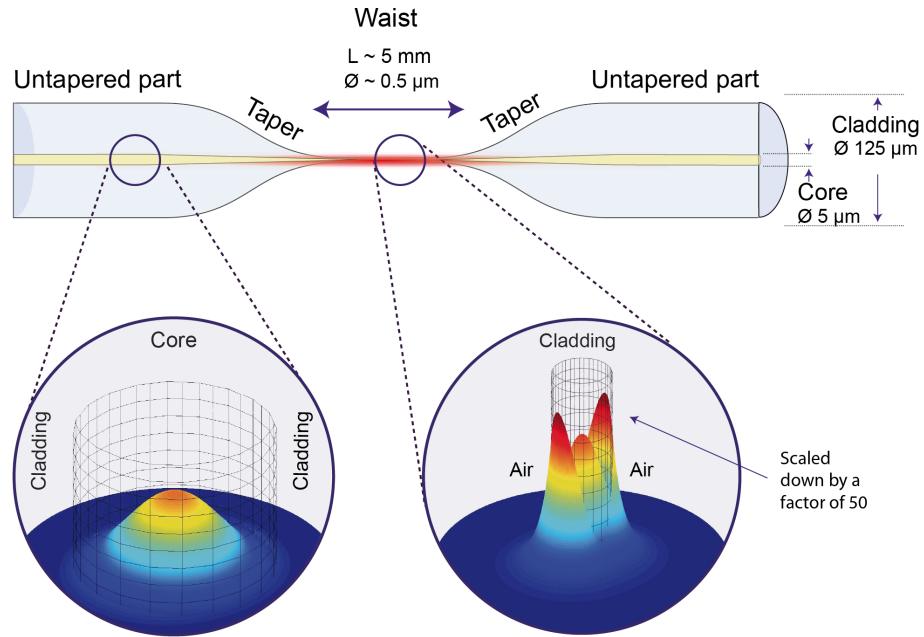


Figure 2.2: A: An optical microfiber consists of an unprocessed standard part, the taper where the diameter changes and a thin part (waist). B: Light travelling through the waist is guided mostly outside of the fibre in the evanescent field.

The intensity in the evanescent field is comparable to the intensity of a tightly focussed free-space beam. However, while in free space the focus depth is only on the order of the wavelength, in case of an OMF tight confinement is kept over the whole waist length. Currently the waist length on the order of 10 mm can be reliably obtained, meaning 10^4 increase of the focus depth. This makes OMFs a suitable tool for light-matter interaction experiments.

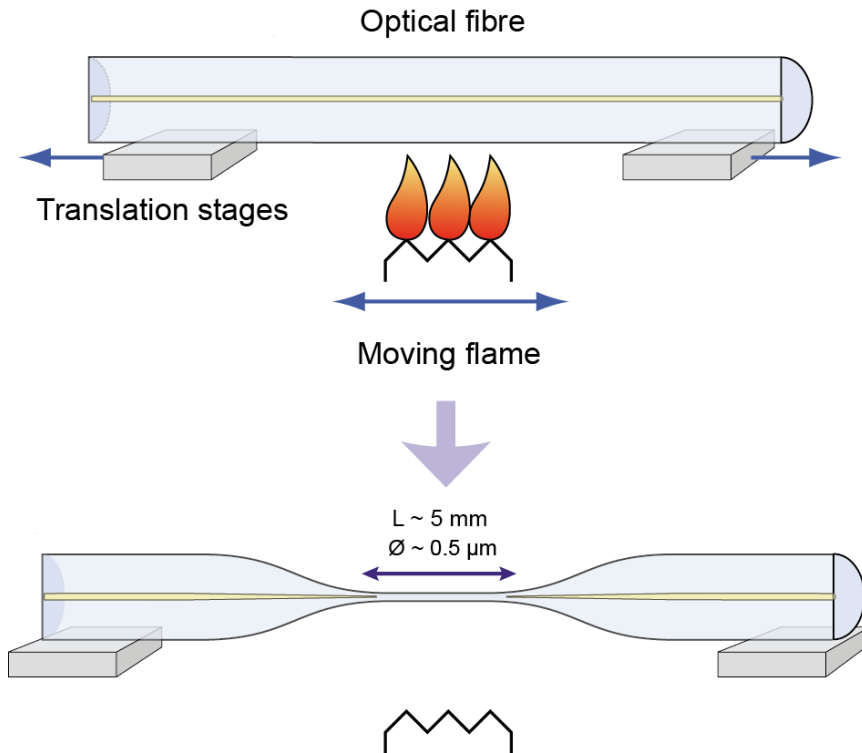


Figure 2.3: The OMF is pulled from a commercial fibre. Two translation stages pull the fibre apart while it is softened by a flame.

2.2 Microfibre manufacturing

To manufacture an OMF the “flame-brushing” technique is used [1, 2]. The fibre is heated to the viscous condition and, simultaneously, pulled at both ends. The pulling machine setup (Fig. 2.3) mainly consists of two translation stages and a hydrogen-oxygen flame. The fibre is fixed on the translation stages with two holding magnets on each side. The fibre coating between the translation stages has to be removed so that the uncoated and cleaned part of the fibre can be heated by the burner. While soft, the fibre is stretched to a desired waist diameter. The translation stage also moves the fibre relative to the flame. The increased effective flame width allows better control of the taper profile than a static flame. The movement of the stages is computer controlled and enables a theoretical precision of $\pm 5\%$ in diameter [3].

The decision on the desired waist diameter depends on the application of an OMF sample. Our Ti:Sapphire-laser operates between 840 nm to 1020 nm. The necessary waist diameters to generate third harmonic light in the first modes (HE_{12} , TM_{31}) can be calculated. They are in the range of 350 to 450 nm (see Fig. 2.6).

For measurements with e.g. light-matter interaction, an intense evanes-

cent field at the waist, and hence a thinner diameter, is beneficial. This consideration has to be weighed up against the stability of the OMF in the vacuum chamber.

2.3 Microfibre properties

2.3.1 Light propagation in OMF

Light coupled into the input on an OMF sample (pigtail A) is guided in the fundamental mode LP_{01} to the down-taper. There, the core diameter becomes smaller and the guided mode is transformed. The taper shape is important for its transmission properties. I use shallow slopes which ensures that the core-guided mode LP_{01}^{core} is transformed adiabatically into the cladding-guided mode $LP_{01}^{\text{cladding}}$ [4].

In the waist of an OMF the core diameter has become insignificantly small and light is guided by the cladding air interface (see also Fig. 2.2). In a mathematical model the waist of an OMF can therefore be regarded as a glass cylinder surrounded by air. The electric field vector \vec{E} of a mode propagating through it can be written in cylindrical coordinates (r, ϕ, z) as

$$\vec{E}(r, \phi, z, t) = \vec{E}_{\perp}(r, \phi) \exp(i\beta z) \exp(-i\omega t)$$

where $\beta = \omega/v_{\text{ph}} = \omega n_{\text{eff}}/c$, n_{eff} is the effective refractive index, $\vec{E}_{\perp}(r, \phi)$ the transverse electric field distribution, t the time, ω the angular frequency of light, v_{ph} the phase velocity and c the speed of light in vacuum. n_{eff} can be determined by numerically solving the eigenvalue equation for the step-profile fibre, as shown in [5]. The solutions for different diameters and modes are calculated by our Matlab program [6] and plotted in figure 2.5. When the diameter of an OMF becomes smaller, more of the light propagates in the evanescent field in air. Therefore the effective refractive index becomes smaller and closer to the refractive index of air. The same is true for the opposite case, when n_{eff} approaches n_{cladding} for larger diameters of an OMF.

In the up-taper, the light is transferred back into the core. After it has been guided out through pigtail B, it can be analysed with a transmission of over 90%.

2.3.2 Harmonic generation in OMF

The nonlinear properties of standard optical fibres have been studied already [7]. The high intensities in optical microfibres lead to even stronger nonlinear effects. They can be used to generate third harmonic light (*third harmonic generation*, THG), as it was expected due to the non-zero third order nonlinearity of silica ($\chi^{(3)}$) and experimentally observed by Akimov [8] and Grubsky [9]. Also *second harmonic generation* (SHG) has been observed [10, 11]. Its origin could be explained by Lægsgaard as a surface

and bulk multipole $\chi^{(2)}$ effect of the fibre [12], which is formed through a multiphoton process involving pump and SHG light.

2.3.3 Phase matching

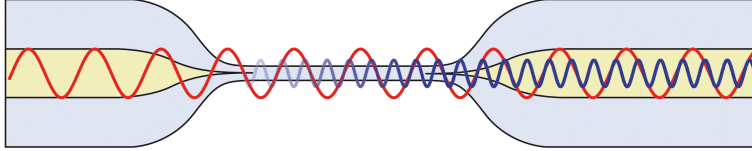


Figure 2.4: Matched phases of fundamental and harmonic light in an OMF.

In order to achieve efficient THG, the phases of the initial and the harmonic waves have to be equal along the whole waist (phase matching, see Fig. 2.4). Due to material dispersion the refractive index increases for shorter wavelengths (considering the same mode). $n_{3\omega}$ or $n_{2\omega}$ respectively, would always be greater than n_{ω} . Hence, phase matching can only be achieved with two different modes. With $v_{\text{ph}} = c/n_{\text{eff}}$ the phase matching condition follows:

$$n_{\text{eff, fundamental}} = n_{\text{eff, harmonic}}$$

These phase matching points can be calculated as described above. As shown in the example in figure 2.5, the fundamental mode of the initial wave has several interception points with higher modes of the third harmonic wave at different fibre diameters. For different wavelengths phase matching occurs at different diameters. Calculating all the interception points for many different wavelengths enables us knowing the phase matching wavelengths of different modes for a given fibre diameter (Fig. 2.6).

This effect can also be used to determine the waist diameter experimentally: The third harmonic and/or second harmonic response strength is measured for different wavelengths of the exiting fundamental. The maximum THG signal corresponds to the waist diameter [13].

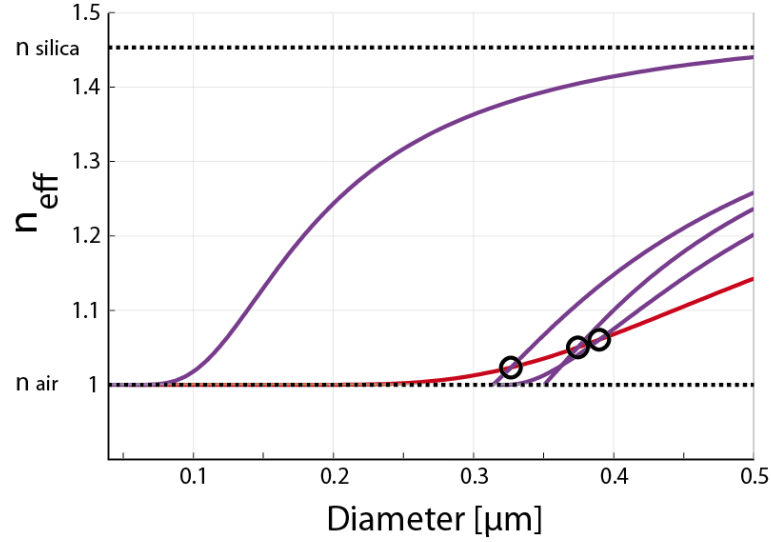


Figure 2.5: Effective refractive index for different modes depending on the waist diameter. The red line is the fundamental mode at 852 nm (ω), the violet lines show higher modes at 283 nm (3ω). The thinner the waist diameter, the closer n_{eff} to n_{eff} of air (more light is guided outside the fibre).

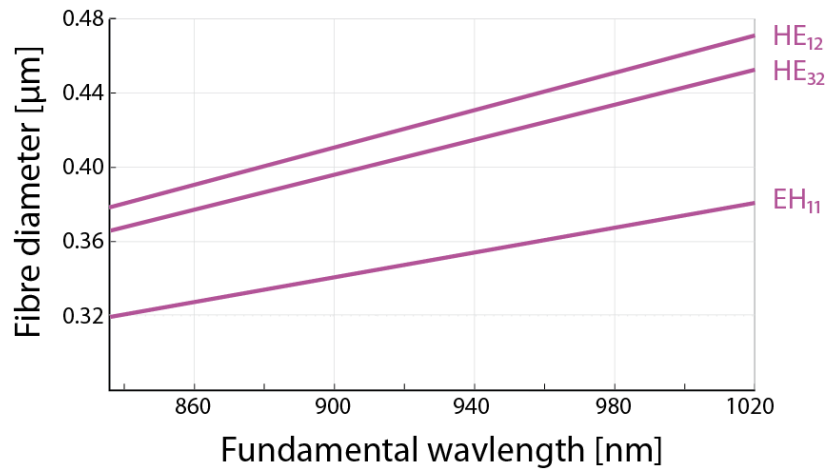


Figure 2.6: From calculating all the phase matching points one can obtain a relation between the harmonic wavelength and the waist diameter.

Chapter 3

Caesium

The high intensities in the evanescent field outside of the OMF (see section 2.1) can be used to generate efficient third harmonic light if a material with a high third order susceptibility is present around the OMF. Caesium gas has been used already to generate third harmonic light with a high intensity free space beam [14]. It is therefore a promising candidate for THG with an OMF.

The presence of caesium itself can be detected, using the OMF for spectroscopy: light in the evanescent field outside of the OMF is absorbed due to electron transitions in the caesium atom which can be detected in an absorption spectrum.

3.1 Nonlinearity of caesium

Most nonlinear optical effects can be described as a frequency-mixing process. If the induced dipole moment of the material responds to an applied electric field E , this dipole moment per unit volume $P(t)$ in a medium can be written as

$$P(t) \approx \chi^{(1)}E(t) + \chi^{(2)}E^2(t) + \chi^{(3)}E^3(t) + \dots$$

where $\chi^{(n)}$ are the n -th order susceptibilities of the medium which describe the polarisability of the material. For frequency tripling a high $\chi^{(3)}$ therefore is required.

3.1.1 Wavelength dependence of $\chi^{(3)}$

The exact value of $\chi^{(3)}$ of caesium strongly depends on the wavelength of the incident light and the amount of atoms. The closer the wavelength to the resonances of caesium, the higher $\chi^{(3)}$ (Fig. 3.1). Within the wavelength range of our Ti:sapphire laser (section 4.1.3), the peak-values of $\chi^{(3)}$ are at the D2 transition of caesium at 852.3 nm and at the D1 transition at

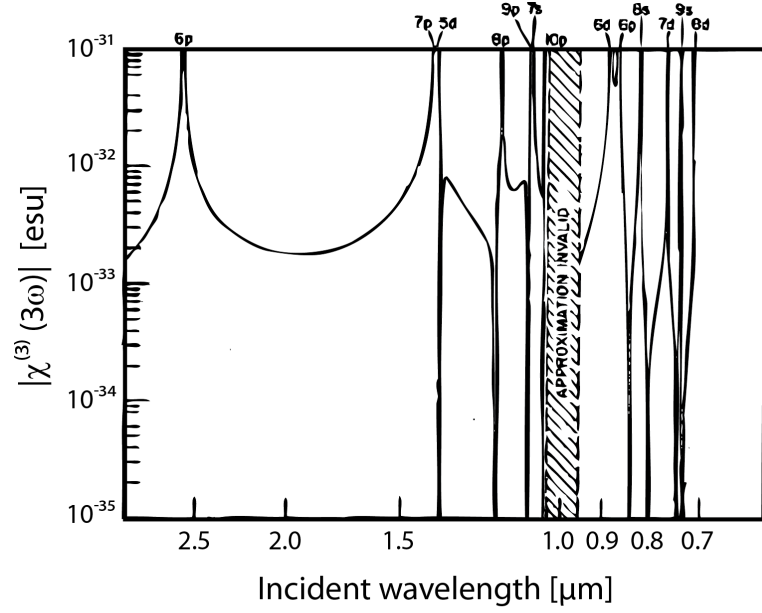


Figure 3.1: $\tilde{\chi}^{(3)}$ of caesium for different wavelengths. [15]

894.6 nm. At these transition wavelengths, light can excite the caesium atoms into higher states and is absorbed. Hence, there is a trade-off between maximising $\chi^{(3)}$ and avoiding light absorption.

3.1.2 Vapour pressure

Fig. 3.1 shows $\tilde{\chi}^{(3)}$ which is $\chi^{(3)}$ of caesium per atom per cubic centimetre. This means the strength of the third harmonic light that is generated with caesium depends also on the number of atoms N in the field of the fibre and therefore on the interaction volume of the light with the atoms.

$$\chi^{(3)} = \tilde{\chi}^{(3)} \frac{NV}{1 \text{ cm}^3}$$

Hence, in order to compare the third order nonlinearity of caesium to other materials, the number of caesium atoms in the evanescent field around the OMF and also the volume in which the field extends have to be known.

The number of atoms depend on the vapour pressure of the caesium and therefore on the temperature. The vapour pressure can be calculated using the vapour pressure model given by [16], which is

$$\log_{10} p_V = 2.881 + 4.165 - \frac{3830}{T}$$

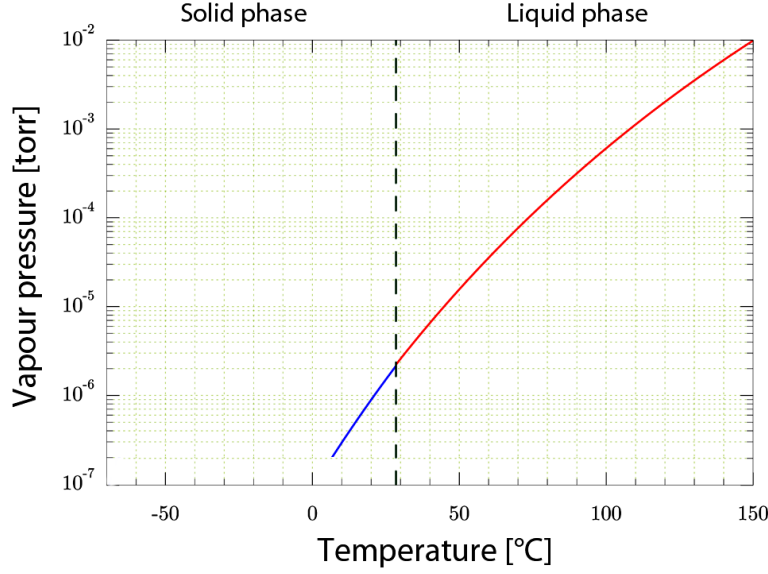


Figure 3.2: Vapour pressure of caesium for different temperatures

where p_V is the vapour pressure in torr, and T is the temperature in Kelvin. The accuracy of this model is given to be better than $\pm 5\%$. A plot of the vapour pressure for different temperatures is shown in Fig. 3.2[17]. For the used value of 70°C in the caesium reservoir, the vapour pressure is $\sim 1 \times 10^{-4}$ mbar.

To estimate the interaction volume V of the light with caesium atoms, the mode-field diameter of the light in the waist is a good guess. The mode-field diameter determines the distance from the surface of the fibre, where the intensity of the light has decreased to $1/e$. For a typical fibre with a $0.44\ \mu\text{m}$ waist diameter, it can be simulated to extend $\sim 300\ \text{nm}$ out of the fibre. The interaction volume therefore can be written as the hollow cylinder

$$V_{\text{mode-field}} - V_{\text{fibre}} = l \cdot \pi (r_{\text{waist}} + 300\ \text{nm})^2 - l \cdot \pi (r_{\text{waist}})^2$$

With a waist length l of $2\ \text{mm}$ the interaction volume is equal to $\sim 1400\ \mu\text{m}^3$.

Knowing the volume and the vapour pressure of caesium, the number of atoms in the field can now be calculated with the ideal gas law

$$pV = Nk_bT$$

where V is the interaction volume, N the number of atoms and k_b the Boltzmann constant. The number of atoms in that volume is calculated to be on the order of 3000 atoms (for a vapour pressure of 1×10^{-4} mbar).

With $\chi^{(3)} = \tilde{\chi}^{(3)}NV/1\ \text{cm}^3$ the effective third order nonlinearity for this specific case hence is 4.2×10^{-13} esu. This is ~ 30 to 40 times larger than the $\chi^{(3)}$ of fuse silica [18, 19].

3.2 Light absorbed by caesium

In order to benefit from the high $\chi^{(3)}$ of caesium, it has to be brought in the evanescent field of the OMF. To check whether caesium is present there, an absorption spectroscopy method is used. The light in the evanescent field of the OMF can be absorbed by caesium at certain well known wavelengths. They are defined by transitions of electrons to higher atom levels of discrete energy. However the absorption spectrum is not discrete but broadened in energy by several effects. This leads to a specific dip" shape of the spectrum. This shape will be studied in theory in this section and will be compared to real measurement data in section 5.

3.2.1 Voigt profile

The frequency that is needed to excite a specific transition in an atom is broadened by mainly two effects. The lifetime of the excited state and the speed of the atoms.

Due to the Heisenberg uncertainty principle, the finite lifetime of an excited state of the atom causes an uncertainty in energy.

$$\Delta E \Delta t \gtrsim \frac{\hbar}{2}$$

with energy E and time t . This broadening of a discrete transition is described with a Lorentzian profile [20]

$$L(\nu) = \frac{\gamma}{\pi(\nu^2 + \gamma^2)}$$

where ν is the frequency and γ is the natural linewidth.

Due to the speed of the free caesium atoms, the absorption profile is also Doppler broadened. Light with a frequency ν below the transition frequency ν_0 can be absorbed by atoms moving (with the velocity v) in the opposite direction than the photons. The optical Doppler effect shifts the frequency of the light seen by the atom

$$\nu = \nu_0 \left(1 + \frac{v}{c}\right)$$

to the transition frequency. Light will be absorbed. The same is true for the opposite case at frequencies above the transition frequency.

The Doppler effect broadens the discrete transitions with a Gaussian profile

$$G(\nu) = \frac{\exp(-\nu^2/(2\sigma^2))}{\sigma\sqrt{2\pi}}$$

where ν is the frequency and σ is the standard deviation.

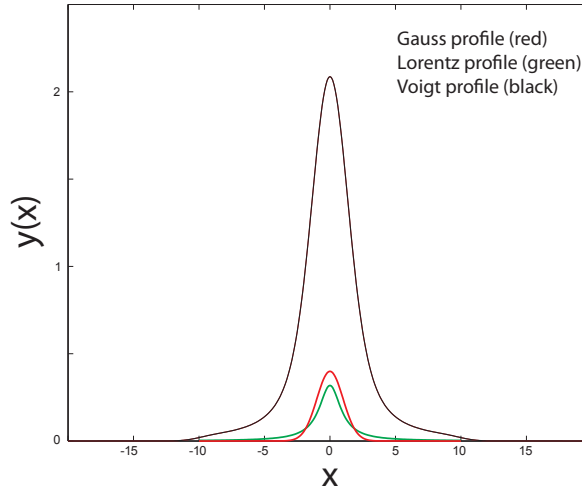


Figure 3.3: Gauss profile (red) with $\sigma = 1$, Lorentz profile (green) with $\gamma = 1$. After convolving the two functions, one obtains a Voigt profile (black).

To describe the absorption spectrum of an atom completely, both effects have to be taken into account. The Gauss profile and the Lorentz profile are convolved (Fig. 3.3), resulting in a Voigt profile. It describes the absorption spectrum of a two level system.

$$V(\nu) = (G * L)(\nu) = \int G(\tau)L(\nu - \tau)d\tau$$

3.2.2 Hyperfine splitting

Real absorption spectra usually do not only consist of one transition as described before. The classical energy levels of an atom are split into a fine structure when considering an electron spin. The energy corrections break the degeneracy of the energy levels and split the spectral lines due to spin-orbit coupling effects. This fine structure is split further into a hyperfine structure due to interactions between the nucleus of the atom and the electrons. Allowed transitions between these levels follow selection rules. Let us consider the D2 transition of caesium.

The D2 transition in the caesium atom is the transition from the $6^2S_{1/2}$ to the $6^2P_{3/2}$ level. These levels are split into hyperfine levels with different total angular momentum F (with $F = I + J$, where I is the nuclear spin and J is the angular momentum of the shell, Fig. 3.4). Transition that do not violate the selection rule $\Delta F = 0, \pm 1$ are allowed.

For this work, a diode laser that pumps from the $F = 3$ level is used. The observable electric dipole transitions therefore are from $F = 3$ to $F' = 2, 3, 4$. All the three transitions are subjected to the Doppler broadening and

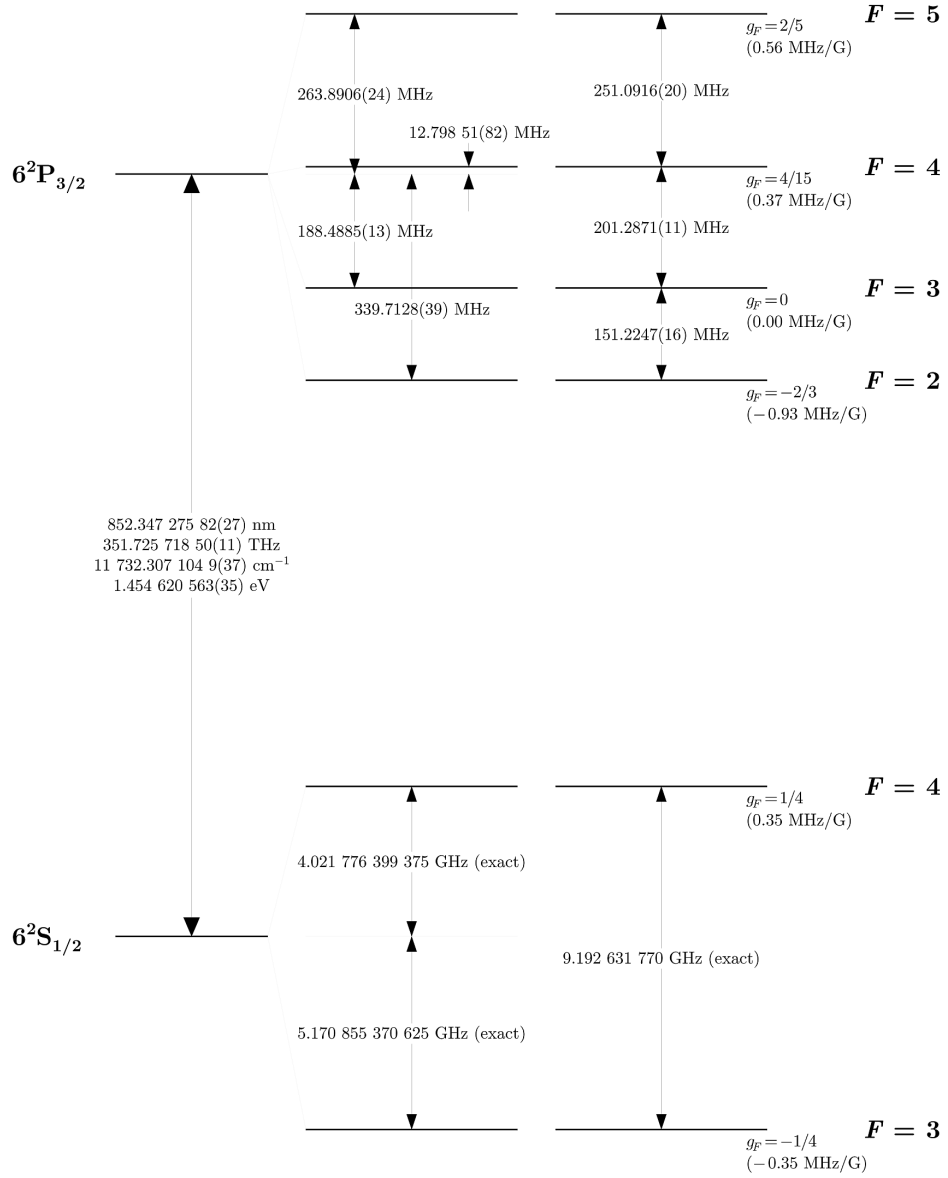


Figure 3.4: Caesium D2 transitions hyperfine structure, with frequency splitting between the hyperfine energy levels [17].

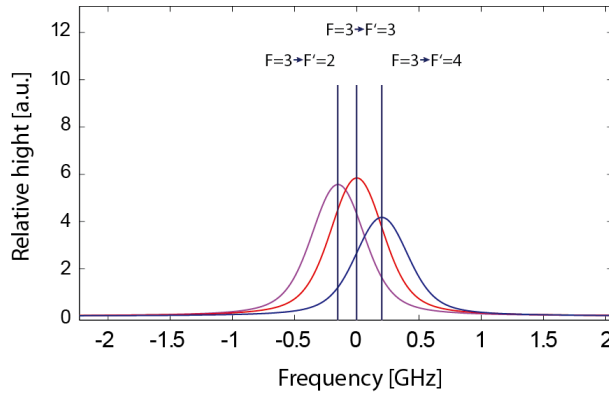


Figure 3.5: Three Voigt profiles of different strength for the three hyperfine transitions $F = 3$ to $F' = 2, 3, 4$ of the caesium D2 line. The frequency scale is centred to the $F = 3$ to $F' = 3$ transition.

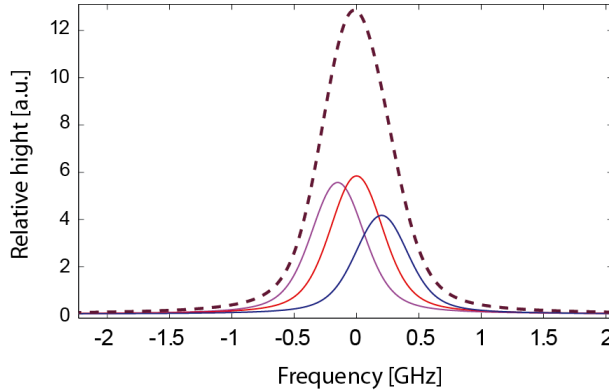


Figure 3.6: Dashed line: The sum of three weighted Voigt profiles determines the theoretical absorption spectrum of caesium at the D2 line, pumped from $F = 3$.

have a natural linewidth. When shone through caesium gas, the absorption spectrum expected from this laser hence consists of three Voigt profiles for the tree transitions. The weight of each profile depends on the transitions strength whereas the position of each profile is determined by the transition energies (Fig. 3.5). These values can be taken from [17].

The plotted sum of these three Voigt profiles is shown in Fig. 3.6.

$$\frac{5}{14}(\nu - 151.2247 \text{ MHz}) + \frac{3}{8}\nu + \frac{15}{56}(\nu + 201.2871 \text{ MHz})$$

with the frequency ν and centred to the $F = 3$ to $F' = 3$ transition. The function is asymmetric due to the different strengths of the transitions and their asymmetric positions in frequency space. It will be used in section 5 to fit measurement data of the caesium absorption.

Chapter 4

Experimental setup

A general overview of the setup that was used to measure THG in different atmospheres and to detect caesium, is given in Fig. 4.1. A light source is coupled into the OMF. The thin part of the sample is installed in a vacuum chamber. The output of the fibre is connected to a detection part, where the power or a spectrum can be measured. Before coupled into the OMF, the light source passes a beam sampler. The second beam can be directly coupled into the detection part. This enables comparing the signals before and after the fibre sample.

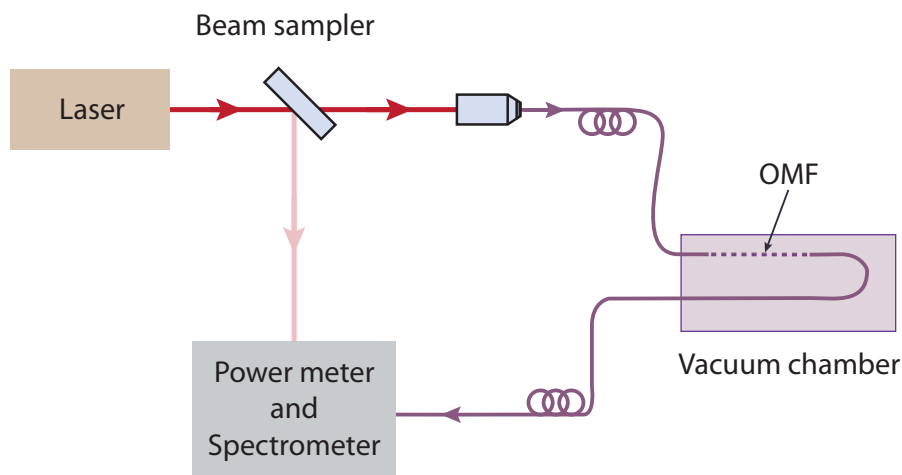


Figure 4.1: General setup with light source, a fibre sample in a vacuum chamber and a detection part.

4.1 Apparatus

4.1.1 Vacuum system

The main experimental part of this work is a vacuum chamber. All of the measurements I have done take place in this chamber. It enables working with the fibre sample in different atmospheres and pressures.

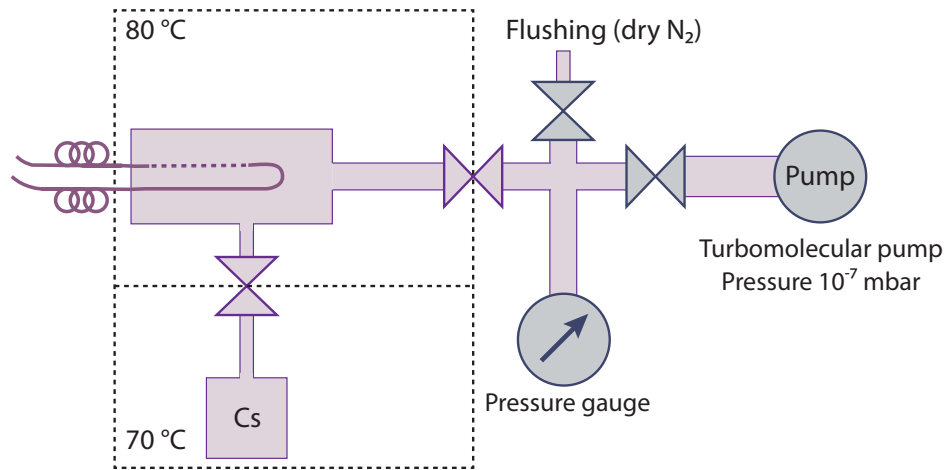


Figure 4.2: Vacuum chamber with a pump part, the main part (with a fibre sample) and a caesium reservoir.

In order to work with caesium gas, the chamber has to fulfil certain requirements. A separable, heatable caesium reservoir with a caesium ampoule is needed to obtain the gas. The distribution area of this reactive chemical should be reduced, the gas should particularly not come in contact with the pump. Also it should be possible to change the fibre samples by opening the chamber. By doing so, caesium must not react with air or water. Hence, the vacuum chamber is split into three main parts: a pump-ventilate part, a part with a fibre sample inside (main part) and a caesium reservoir (Fig. 4.2).

To achieve a high caesium vapour pressure and maximise the amount of caesium gas in the chamber, as much air as possible has to be pumped out. Hence, ultra high vacuum (UHV : $< 10^{-7}$ mbar) is the pressure range I used. For UHV all the vacuum components have to be ConFlat (CF). CF flanges are made of stainless steel and can be used up to 500 °C . Caesium is very aggressive and reacts with copper gaskets that are usually used to connect CF parts. Therefore silver-coated copper gaskets have been used with the vacuum parts that come in contact with caesium. The silver is not etched by the caesium.

The heart of the pump section is a turbo-molecular pump (Oerlikon

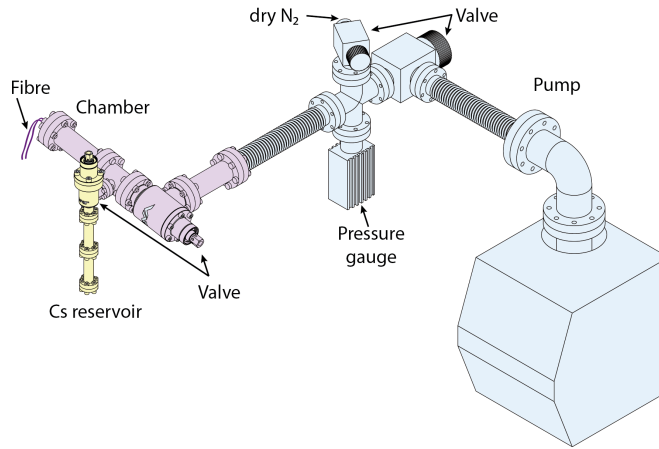


Figure 4.3: A CAD drawing of the complete vacuum system.

Leybold PT70 F-compact). It reaches pressures down to 10^{-8} mbar. The pump stands on the laboratory floor, as opposed to the other elements that are fixed on an optical table. This reduces vibrations which could influence the measurements. For the same reason, the intake flange of the pump is connected to the rest of the setup with a flex hose. The pump can be disconnected with a standard UHV valve.

The main part of the apparatus is where the fibre samples are installed with the spread fixation. It is closed with a CF-Swagelok adapter with a Teflon ferrule used as a feedthrough (see Section 4.2.2). In order to replace the fibre sample, the chamber has to be opened. Therefore the caesium reservoir needs to be separated from the main part. Standard UHV valves can not be used for this purpose. They contain rubber gaskets which are etched by the caesium. Instead an all-steel valve (VAT series 57.1) is installed. It can withstand operation temperatures up to $350\text{ }^{\circ}\text{C}$ and can be used with aggressive gases like caesium.

The main part is connected to the pump part with another all-steel valve (VAT series 57.1) in order to protect the pump and the pressure gauge (IONIVAC ITR 90) from caesium. While working with caesium gas, this valve is always closed. The pressure inside the main part can than not longer be measured by the pressure gauge.

The caesium part itself is made of two nipples. A cracked caesium ampoule is located at the bottom of the lower nipple. Since caesium is very reactive with air, this part should always be kept under vacuum.

In order to work in a nitrogen atmosphere and also to ventilate the chamber, a nitrogen supply is connected. To not spoil the chamber with water, the nitrogen I am using passed through an drying cartridge (MicroTorr In-line by Pure Gas Products).

A full 3D CAD drawing of the vacuum system is shown in Fig. 4.3.

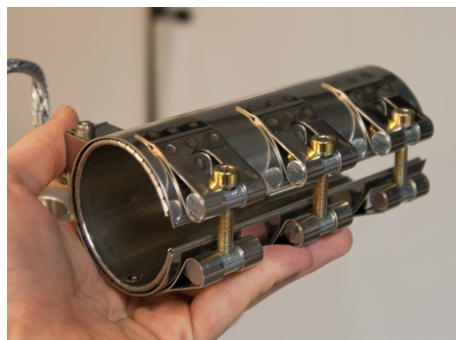


Figure 4.4: A small element of Mickenhagen's DAW heating jacket used for the caesium reservoir.

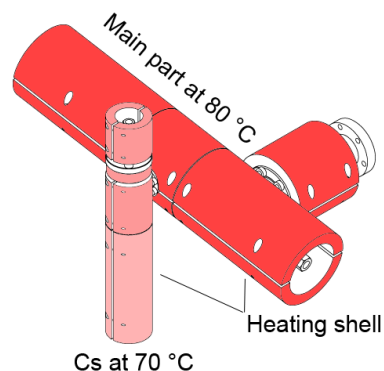


Figure 4.5: Heating shell around the vacuum chamber with temperature settings.

4.1.2 Heating system

To obtain caesium in a gaseous form, a heating system is needed. The caesium will always condense at the coldest point, therefore the main part of the chamber has to be kept at higher temperatures than the caesium reservoir. Hence, the heating system needs to provide the possibility to control the temperatures separately for each part of the chamber (main part, caesium part). For the same reason the heating should provide an stable and even distribution. It ensures that the set temperatures are kept at any point of the chamber and no caesium will condense anywhere but in the reservoir. Like this, caesium will only be present in the main part as a gas.

Mickenhagen's DAW is the heating system of our choice for this purpose (Fig. 4.4). The full heating setup consists of aluminium shells, heating jackets, aluminium foil and sensors connected to a controller.

The custom-made aluminium shell is attached to the vacuum parts for a smoother heat distribution and to even out the irregularities of the nipples (difference in diameter between tubes and flanges). It is attached to the nipples and valves such that they are covered completely (Fig. 4.5).

Five full area metal heating elements are slid over the shell. They cover the chamber nipples of the main part and the caesium part completely. Unlike a heating wire, the full area jackets contain no splintery insulation fibres. Hence, frequent opening of the chamber is possible without residual fibres getting into the vacuum system. Three larger jackets are used to heat the main part of the chamber. Two more cover the caesium part. Each separate jacket is computer controlled separately.

To heat up the chamber, the final temperature is set with a heating controller. Also the heating speed is important: different materials have

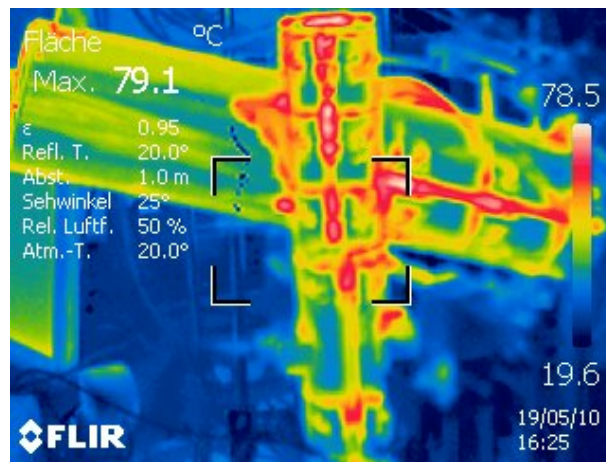


Figure 4.6: Infrared photo of the hot vacuum chamber 80 °C.

a different coefficient of thermal expansion. Therefore the copper-gasket steel-nipple connection can become leaky when the temperature changes too quickly. The all-steel valves that I am using are specified to 1 °C per minute. Hence, for this work I always used the heating speed 0.7 °C per minute, to not risk problems with the valve. Also VAT limits their valve to a temperature gradient (between input and output flange) of 70 °C.

The temperatures around the jackets can be very different depending on where it is measured. At the edges, or next to a slit, the temperature can be up to 20 °C lower than inside the shell. To measure the temperature reproducibly at the same point and with the best accuracy, the sensors are therefore fixed. I installed one sensor for each heating jacket at the inside wall of the shell. They are fixed with clamps and then connected to the heating controller. The heating current for each jacket is adaptive to the measured temperatures of the sensors.

In an infrared photo (Fig. 4.6) one can see that the heat is mainly lost at the slits of the heating jackets. For a better efficiency and an even heat distribution, the jackets are therefore covered with three layers of aluminium foil.

The cooling down process also is computer controlled. However, the steel nipples and the aluminium shell store a lot of heat. Therefore no action has to be taken by the controller to provide cooling down with 0.7 °C per minute. In fact all the parts cool down much slower. In doing so, the main part cools slower than the caesium part due to its larger volume. This is of critical importance in case of an electrical power breakdown. The caesium reservoir will cool down faster than the main part automatically and no caesium will condense inside the main part of the chamber.

After a full heating cycle to 120 °C with a Teflon ferrule feedthrough, the chamber stays tight. A final pressure of 5.3×10^{-7} mbar was reached after

baking out for two days.

4.1.3 Optical setup

The used light sources depend on the experiment: A tunable Ti:sapphire laser for THG (Spectra Physics Tsunami 850 nm to 1000 nm, pumped with Spectra Physics' Millennia Pro 15sJ), a diode laser scanning the D2 line of caesium used for the caesium detection (Toptica DC110), or a white light source (Avantes AvaLight-HAL) for spectra analysis have been used for this work.

The detection part consist of either a silicon power meter (Thorlabs PM100D with S120VC head), a thermal power meter (Thorlabs PM100D with S310A head), or a photomultiplier (Hamamatsu H5784-03), depending on the measured light powers. For spectral analysis an Avantes spectrometer (AvaSpec 3648-UA-25-AF) was used.

A more detailed description of the optical setup is given before every experiment.

4.2 Using fibre samples

4.2.1 Types of optical fibres

Since and OMF it is pulled from standard optical fibres, one has to choose between a great many of different fibres that are available on the market. They differ in many parameters like e.g. material and diameter (see table 4.1). The parameters determine the field of application of the optical fibre.

In order to do experiments with caesium around the D-lines, my fibres need to transmit infrared light between 840 nm to 1020 nm (the working range of the Ti:Sapphire laser). For efficient harmonic generation, all the light also has to be guided in the LP_{01} mode (see section 2.3.3). Hence, the fibre needs to be single mode for these infrared wavelengths. Fibercore's SM800-5.6-125A fibre matches these requirements.

With the infrared working range between 840 nm to 1020 nm, third harmonic light between 280 nm to 340 nm can be generated in the waist of an OMF made of SM800. The exact wavelength of the generated UV light depends on the diameter of the waist. Since the core of SM800 is germanium doped, it absorbs UV light. SM800 can therefore not be used to guide the UV light to the output of the sample (pigtail B). Hence, a pure silica core UV transmitting fibre like Ceramoptec's UV50-125A has to be connected permanently after the up-taper of the OMF.

The two types of fibre have to be connected before the pulling process, using a *fusion splicing* machine (Fujikura FSM-30S). The fibre lengths are

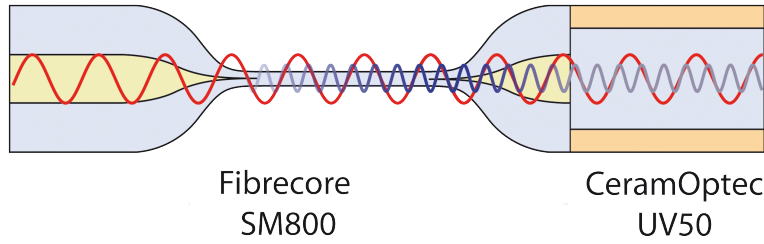


Figure 4.7: An OMF spliced from SM800 and UV50. Third harmonic light is generated in the SM800 waist and can be guided out by UV50.

choose in a way that after pulling the whole up-taper, down-taper and waist will be made of SM800. Pigtail B will consist of UV50 fibre.

The spliced fibre is pulled with the pulling machine as described in section 2.2. A sketch of an often manufactured spliced OMF sample is shown in Fig. 4.7.

4.2.2 Fibre in the vacuum chamber

Fibre holder

In order to store a samples, it is permanently fixed on a holder. Small droplets of UV cured glue hold the uncoated pigtail of the OMF right after the taper regions (see Fig. 4.8). A cover is fixed around the holder. The pigtails are clamped additionally to the cover to grant additional protection.

Holder in the chamber

To have caesium reach the waist of the OMF, the sample cover is removed before it is put into the vacuum chamber. Since the fibre is uncoated in holder, it can easily break when touching the metal edge. Therefore I improved the sample holder with an elongation piece, which is screwed to one

| | | Fibercore SM800 | Ceramoptec UV50 |
|--------------------|----------|-----------------------|-------------------|
| Type | | Single mode | Multimode |
| Core | diameter | 5.6 μm | 50 μm |
| | material | Ge-doped fused silica | Pure silica |
| Cladding | diameter | | 125 μm |
| | material | Pure silica | F-doped silica |
| Coating | diameter | | 250 μm |
| | material | | Dual acrylate |
| Cut-off wavelength | | 660 nm to 800 nm | < 1020 nm |

Table 4.1: Properties of the fibre types used.

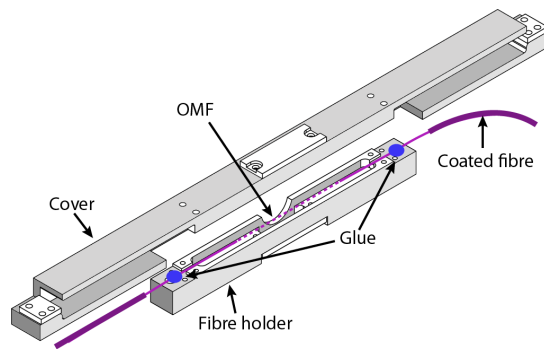


Figure 4.8: Microfibre fixed in a holder with glue and protected by a cover.

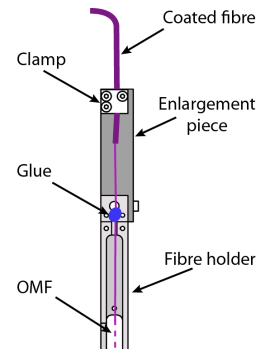


Figure 4.9: Enlargement piece enabling bending of the fibre in the chamber.

end of the holder. It makes it possible to fix the fibre additionally with a clamp through the coated part (see 4.9). Bending the pigtail to install the sample into the chamber becomes unproblematic.

In order to fix the holder inside the nipple of the chamber, it is connected with a spread fixation. The fixation consists of two plates connected with screws. The fixation can be spread apart with the screws until the distance between the plates is big enough to tightly fix the holder inside the nipple (see Fig. 4.11).

Fibre feedthrough

Since the optical setup is not inside the vacuum chamber, the fibre pigtail is fed out the chamber in order to do the measurements. No heat-resistant, commercial connector exist for this purpose. Instead a Swagelok adapter with a ferrule is used.

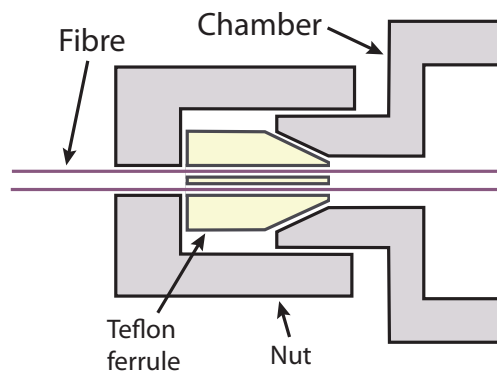


Figure 4.10: Teflon ferrule used as a fibre feedthrough.

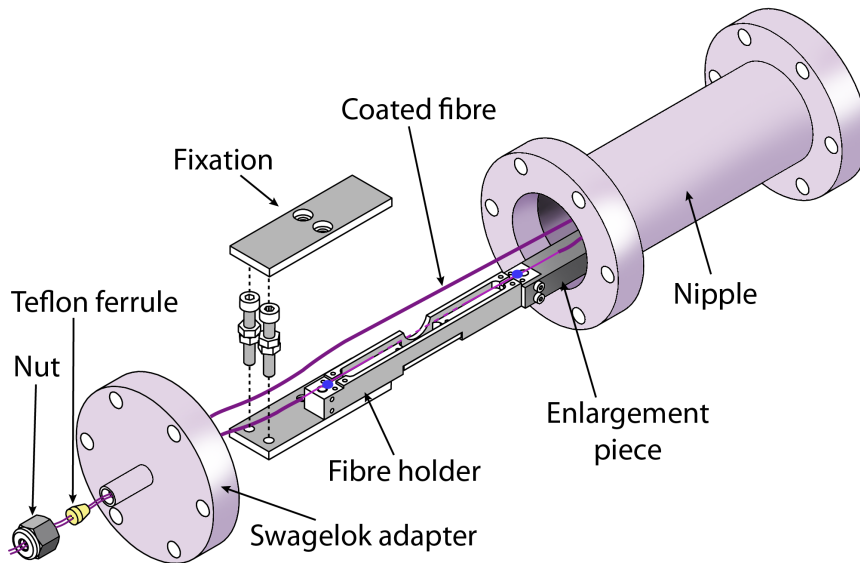


Figure 4.11: Sample installed in the vacuum chamber. A spread fixation holds the sample inside the nipple. The chamber is closed with a Swagelok adapter and a Teflon ferrule used as a feedthrough.

Standard metal ferrules require metal coated fibres. Since the types of fibres needed for my experiments are not available with a metal coating, another type of ferrule is used. This ferrule is a home-made solid Teflon cylinder that matches the dimensions of commercial ferrules [21] (Fig. 4.10). Two holes are drilled into the Teflon to feed the fibres. The hole diameter is chosen such that the coated fibre can be threaded through and sealing of the chamber is possible. A hole diameter of $300\ \mu\text{m}$ has turned out to be a good choice for the $250\ \mu\text{m}$ diameter coated fibre pigtailed. After screwing the Swagelok nut on the adapter, the soft Teflon presses directly on the acrylate fibre coating making the chamber tight.

The inexpensive ferrules can be easily manufactured and replaced after each opening of the chamber.

4.3 Caesium in the chamber

In most of my experiments caesium gas is used. In this section the method of how to obtain caesium gas in the chamber and where to pay attention while working with caesium is demonstrated.

With only one valence electron, caesium is a very reactive alkali metal and has to be handled with care. In air, caesium can spontaneously start burning. In water it explosively reacts to caesium hydroxide ($2\text{Cs} + 2\text{H}_2\text{O} \rightarrow 2\text{CsOH} + \text{H}_2$) which is a very strong base and can etch silica [22]. Hence,

it is stored in evacuated ampoules. The melting point of caesium is very low (28.7°C) such that touching the ampoule causes the caesium to melt already.

By fluorescence with a caesium-resonant laser the authenticity of the ampoule has been checked. Then the cracked ampoule was installed inside the caesium reservoir of the vacuum chamber. To avoid liquid caesium in the workspace, the ampoule has been cooled down with liquid nitrogen before it was cracked. Once inside the chamber, it was pumped out immediately to avoid reactions with air. The vacuum has to be kept all the time. Therefore the caesium reservoir is always disconnected with a valve during the fibre samples are changed.

To further avoid reactions of the caesium with water inside the chamber, it is always baked out after new fibre samples are installed. This reduces the amount of water inside the chamber. The caesium reservoir itself can never be baked out, since at high temperatures there is already caesium vapour present which can spoil the pump. This means it is either possible to pump out the chamber (while baking) or having the caesium reservoir open. Due to the fact that the caesium reservoir is not baked out, large amount of caesium will remove all the residual water by itself in a minor chemical reaction.

Once the chamber is baked the pump is disconnected and the caesium reservoir can be opened to obtain a caesium vapour around the OMF. When the OMF needs to be replaced, the caesium has to condense back into the reservoir first. Hence, the caesium reservoir is cooled down faster than the chamber. Once everything has cooled down, the reservoir is disconnected and the OMF can be replaced by opening the Swagelok adapter.

4.4 Challenges and limitations

To obtain a dense caesium vapour, the temperature needs to be increased (see section 3.1.2). The heating system and the Teflon ferrule can be used up to 300°C . Still there are factors that limit the operation temperature of the chamber.

Most of all the fibre coating: the dual acrylate is only specified up to 80°C . I tested the chamber up to 120°C and it stayed tight. The feedthrough was not affected by the softer coating. Still the acrylate starts degrading. It has been observed after replacing the fibre that it had a brownish look, whereas burned coating material also trickled on the walls of the chamber. There are fibres with a different coating material specified for higher temperatures, but not this specific single mode infrared fibre with a silica core that I need for my experiment (see section 4.2.1).

Another limiting factor is the thermal expansion of the fibre holder. With

a expansion coefficient of $\alpha = 23.2 \times 10^{-6} \text{ K}^{-1}$, the aluminium expands by

$$\Delta l = l_0 \alpha \Delta T = 350 \text{ } \mu\text{m}$$

while heating the holder by $\Delta T = 100^\circ$ (where $l_0 = 15 \text{ cm}$ is the length of the holder). The expansion coefficient of silica on the other hand is much lower: $\alpha = 0.5 \times 10^{-6} \text{ K}^{-1}$. This means that during heating the fibre is stretched and can rip. To avoid this problem, I unstretched the samples after pulling, using the translation stages of the pulling machine. Like this the OMF slightly sags when it is glued to the holder at room temperature, but becomes straight in the hot chamber environment.

Chapter 5

Caesium detection

Within this work, third harmonic light is generated with OMFs. In order to know whether the THG is indeed due to caesium, it is crucial to know if caesium atoms are present in the evanescent field of the OMF. The caesium can be detected using the method of absorption spectroscopy: light coupled into the OMF will be absorbed if its frequency hits a transition of the caesium atom. The energy is absorbed to excite electrons into a higher state. Therefore a decrease in the light transmission will be visible for that frequency. If this absorption peak can be detected at the very characteristic D1 or D2 line wavelengths of caesium, the presence of free caesium atoms around the fibre is proven.

5.1 Absorption spectroscopy

The absorption spectrum of caesium is on the order of 1 GHz. A spectrometer or an optical spectrum analyser have not the sufficient resolution to detect this narrow absorption dip. Therefore a single-frequency laser is used to detect the caesium absorption by scanning the laser frequency on the Gigahertz scale while measuring the transmission.

5.1.1 Setup

A diode laser (Toptica DC110 at 22.1 °C and 48 mA) with a spectral width of only ~ 100 kHz, scans over the frequency range of the D2 line of caesium (pumping from the $F = 3$ state). The frequency is selected with a movable, piezo-controlled diffraction grating at a scanning speed of 30 Hz. The frequency of the laser has to be tuned mode-hop over a larger range than possible with the grating. Hence, the diode current also has to be modulated. This current modulation enables scanning the full caesium D2 line, but also changes the power of the beam continuously.

In order to detect caesium around the waist of the OMF, the setup

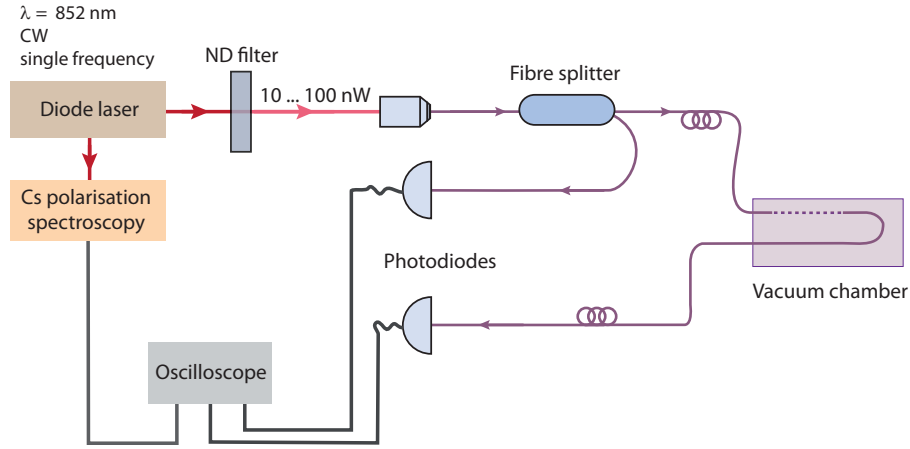


Figure 5.1: Setup for caesium absorption spectroscopy

shown in Fig. 5.1 is used. To determine the absorption due to caesium, the light power before and after the sample has to be compared. Therefore the beam is first coupled into a fibre splitter. It splits the beam with a ratio of 7.125:1. The lower power output of the splitter is connected to the OMF in the vacuum chamber, the other output is directly connected to a amplified photodiode (homemade model with $1 \text{ M}\Omega$ resistor). Its voltage is used as the power reference signal. The output of the OMF is connected to a second amplified photodiode of same type to detect the power after the fibre.

The photodiode voltages are measured by an oscilloscope. Since the repetition rate of the scan is 30 Hz, the electronic high-frequency noise can be cut-off from the measurement using a low-pass filter. I used a $1.2 \text{ k}\Omega$ resistor with a 4.7 nF capacitor to cut-off frequencies higher than 28 kHz.

5.1.2 Frequency calibration

In order to detect caesium around the OMF with the D2 transition, the laser diode has to be tuned to the correct transition frequency. Since my photodiodes can only detect only the transmitted light power in time due to the scanning laser, a caesium reference is needed to know the exact frequencies. Hence, one part of the beam (Fig. 5.1) is shone through a caesium reference cell. With a saturation spectroscopy setup a characteristic caesium absorption spectrum can be detected from that cell if the proper frequency has been hit. The saturation spectroscopy setup is part of a polarisation spectroscopy setup that was already used in use in our group. Therefore it was easy to access and will not be further described here.

To convert the measured data into frequency-space, the absorption spectrum from the caesium reference cell is used. Since the saturation spectroscopy is Doppler-free, Lamb dips are visible in the spectrum of the refer-

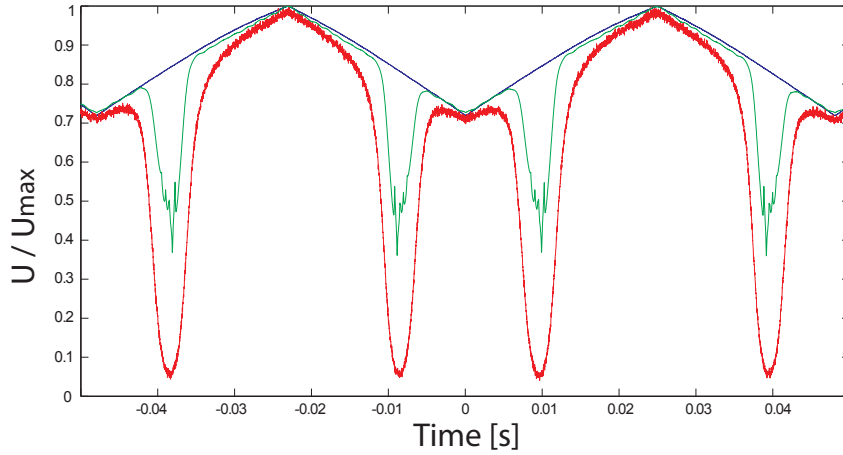


Figure 5.2: Absorption spectrum measurement versus time. With power after sample (red), power reference (blue), and Doppler-free calibration signal (green).

ence cell beam (see Fig. 5.2). They almost correspond to the hyperfine transitions mentioned in Section 3.2.2 with an error of less than $\pm 2\%$ (checked with the polarisation spectroscopy setup). The frequencies of these hyperfine transitions are well known (see Fig. 3.4). Therefore the Lamb dips can be used to convert the time axis of the measurement into a frequency axis.

5.1.3 Measured absorption

Fig. 5.2 shows a typical absorption measurement taken with the OMF. In this measurement, the caesium reservoir was open for two weeks at 70°C . The average power before the OMF is 20 nW . The green line shows the calibration absorption spectrum from the caesium reference cell. The blue curve displays the power reference before the OMF. The red curve is the power after the OMF with a caesium absorption dip visible. All the curves have a slope due to the current modulation of the laser diode.

It is crucial to carefully subtract the dark voltages of the photodiodes to ensure that the powers are comparable. To process the data and analyse the shape of the absorption spectrum, the normalised power after the sample (red) is divided by the normalised power reference (blue). By this manner it is possible to compensate the changing power of the laser.

The obtained normalised absorption spectrum in frequency space can be compared to the theoretical model described in section 3.2.2. This fit varies only the width of the Doppler broadening (Gaussian σ) and the natural linewidth (Lorentzian γ), as well as the relative transition strength of the spectrum (y -position). The position in terms of frequencies (x -position) is fixed due to the well known transitions.

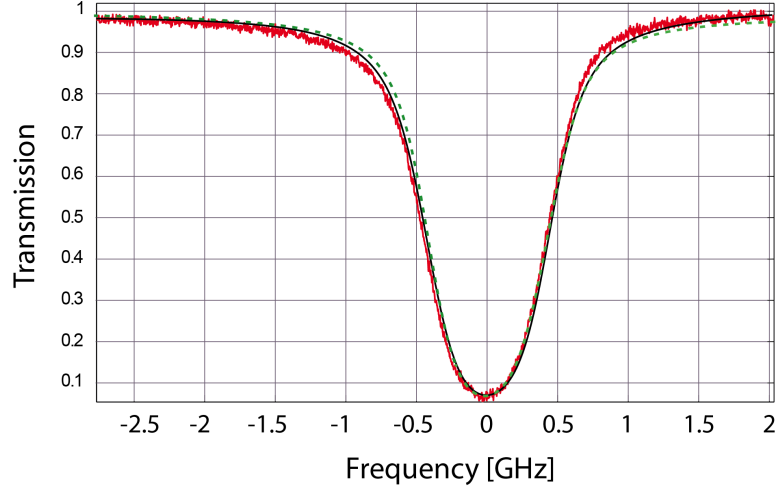


Figure 5.3: Caesium absorption spectrum measurement compared to two theoretical model. Green line: without power correction, black line: with power correction.

The resulting fit curve is shown in Fig. 5.3 (dashed green line) and meets the theoretical expectations satisfactory. However, it does not match the asymmetry in the shoulders of the spectrum. Considering the frequency-depending power modulation explained in section 5.1.1, the incident laser power for lower frequencies is lower than for higher frequencies. In addition, the higher the power, the more caesium atoms around the fibre waist can be excited. In this case more atoms become saturated and cannot absorb light. Therefore the transmission through the fibre will increase with higher powers.

Since the lifetime of the excited state determines when an atom is able to absorb another photon, this power effect affects the Lorentzian part of the Voigt profile. The Gaussian part depends only on the temperature. Adding this power factor into the Lorentzian part of the Voigt profile as described by [23] gives

$$L(\nu) = \frac{\gamma}{\pi(\nu^2 + \gamma^2 \cdot (1 + \psi \cdot \Delta P(\nu)))}$$

with $\Delta P(\nu)$ the known power modulation and ψ a scaling factor (as a new fit parameter).

The power adapted fit is shown in Fig. 5.3 with a black line.

The standard deviation of the Gauss profile (the fit parameter σ) should coincide with the theoretical Doppler broadening at 80 °C (the temperature in the chamber).

$$\sigma_{\text{theoretical}} = \frac{\nu_0}{c} \sqrt{\frac{k_b T}{m}} = 174 \text{ MHz}$$

where ν_0 is the transition frequency of 351.73 THz, c is the speed of light, k_b is the Boltzmann constant, T is the temperature in the chamber (353 K) and m is the mass of a caesium atom (2.21×10^{-25} kg).

The width of the Lorentzian profile (the fit parameter γ) should coincide with the natural linewidth of caesium D2 line.

$$\gamma_{\text{theoretical}} = \frac{1}{2\pi\tau} = 5.2 \text{ MHz}$$

where τ is the lifetime of the excited state (30.4 ns[17]).

The widths obtained from fitting different measurements taken at different days (meaning with a different amount of caesium atoms around the OMF) are averaged:

$$\sigma = 178(6) \text{ MHz}, \quad \gamma = 65(10) \text{ MHz}$$

where the error is the determined by the standard deviation from the mean value.

The results show that the theoretical Doppler broadening is described well by the fit. However, the measured natural linewidth is ten times larger than the theoretical values. Hence, additional broadening effects might affect the measurement. They are discussed in the next section.

5.1.4 Influences on the dip shape

The theoretical model of the absorption spectrum of the D2 line does not perfectly coincide with the measured data. In particular there still is an asymmetry in the shoulders of the Voigt profile and a much too broad Lorentz width.

This can be mainly due to two effects. First of all the time of flight broadening: The caesium atoms around the OMF have a speed of

$$v = \sqrt{\frac{k_b T}{m}} = 148.5 \text{ m s}^{-1}$$

where k_b is the Boltzmann constant, T is the temperature in the chamber (353 K) and m is the mass of a caesium atom (2.21×10^{-25} kg). Then the shortest possible interaction length of one of the caesium atoms with the evanescent field of the OMF is determined by a direct incident trajectory perpendicular to the surface. Assuming the size that the evanescent field extends from the OMF to be $x = 300$ nm by simulating the 1/e decrease in intensity. Hence, the shortest possible interaction time between the atom and the light is $t_{\text{interaction}} = x/v \approx 2$ ns. This is shorter than the lifetime of the excited state (30.4 ns). The linewidth of the transition in that case is not longer determined by to the natural linewidth, but by the time of flight.[20]. This can explain the deviation in the Lorentzian γ .

Since caesium interacts with the fibre, another broadening effect can occur: the van der Waals broadening. Caesium atoms close to the surface of the fibre are perturbed by van der Waals forces. Their energy is red-shifted by $\Delta E \sim 1/r^6$. Therefore this shift has a larger effect on atoms close to the surface of the fibre but barely on the atoms further away. The asymmetric van der Waals potential hence broadens the absorption spectrum asymmetrically [24, 25]. This effect could therefore explain the asymmetrical deviation in the shoulders of the measured absorption spectrum from the theoretical model.

5.2 Effects of caesium vapour

The presence of caesium is not only noticeable with absorption spectroscopy. Due to the high reactivity of caesium it reacts with the materials used in the vacuum chamber. These reactions are only observable after cooling down the chamber and opening the Swagelok adapter.

After opening the chamber there is a penetrative smell for some seconds. Even though the chamber is flushed with dry nitrogen, this could be a reaction of residual caesium in the chamber with the surrounding air. Also noticeable is the colour change of the fibre coating and the Teflon ferrule. The once transparent fibre coating is shimmering slightly yellow. The inner surface of the Teflon ferrule is dark brown or black. The mentioned effects are not observable when using sample at 80 °C without caesium vapour.

5.3 Characterizing the caesium absorption dip

5.3.1 Absorption with different laser powers

As mentioned in section 5.1.3, the maximal absorption depends on the light power. For higher powers more atoms are saturated and cannot absorb more photons.

This effect can be measured by changing the average laser power coupled into the OMF with neutral density filters (using the same setup Fig. 5.1. The data is taken and analysed as described in section 5.1.3. The maximal absorption value (dip depth) is calculated and plotted versus the power before the sample (Fig. 5.4). This measurement has been repeated several times within 16 days with the caesium reservoir opened permanently. In the result a clear dependence of the dip depth on the power is visible. The absorption of higher powers is lower because the atoms get saturated. The theoretical absorption is given as

$$\text{Absorption} \propto \frac{1}{\sqrt{1 + S(P)}}$$

where S is the saturation factor and P is the power [20].

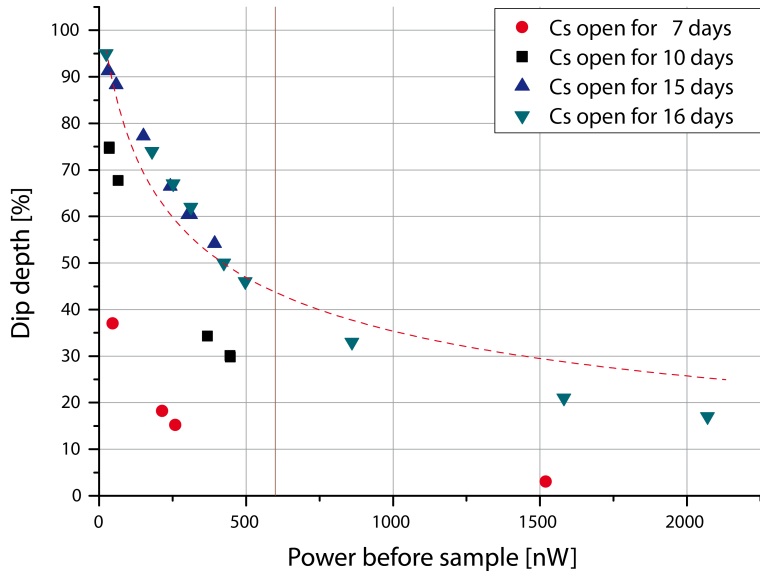


Figure 5.4: Caesium dip depth vs. power at different days.

This easy model function has been fitted to the data and is plotted in Fig. 5.4 with a dashed line ($S(P)$ as a fitting parameter). Since the power distribution in the evanescent field of the OMF is not homogeneous, the measurement does not agree with this theoretical line. The light intensity in the evanescent field depends on the distance from the fibre. There can be intensities high enough to saturate the atoms closer to the fibre. On the other hand, there will always be intensities low enough to be absorbed by caesium atoms further away from the surface. This behaviour has been studied and numerically solved by [25]. This explains the strong deviation of the simple theoretical absorption model from the measured data.

It is as well noticeable that the dip depth shifts upwards. The longer the caesium reservoir is opened, the more atoms are around the OMF and more light is absorbed. This indicates that the amount of caesium atoms is increasing very slowly and is not in an equilibrium even after several days.

5.3.2 Temporal evolution of the absorption

It is important to know when the caesium vapour inside the chamber has build up and the amount of caesium around the fibre stays constant. Therefore the above mentioned temporal effect is studied in more detail. In order to do so, the power before the sample is fixed to 20 nW. The absorption spectrum after the OMF is analysed at different days using the method described in section 5.1.3. The dip depth versus time is shown in Fig. 5.5.

Again a temporal effect is observable (as seen in section 5.3.1). After a

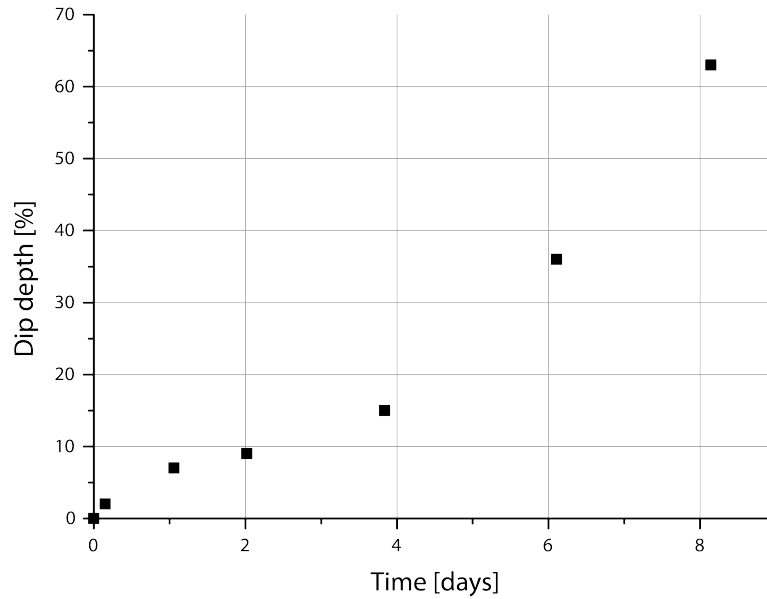


Figure 5.5: Caesium dip depth vs. time with fixed power.

longer waiting time with the caesium reservoir open (at 70°), the dip depth and thus the absorption increases. It is noticeable that I was no able to detect caesium within the first two hours. The increase of the absorption in time seems to have two different slopes. During the first 3 to 4 days, the absorption increases slower than after the fourth day. This could be due to a gettering effect. The first caesium atoms entering the chamber stick to the walls and are chemically adsorbed. Some of the atoms might also react with residual water or the silica of the fibre. Once the walls are covered with a mono-layer of caesium the amount of gaseous caesium increases quicker.

The build up of caesium vapour is not infinite. After about two weeks the transmission trough the OMF drops to below 0.1 percent. This could be due to caesium sticking on the waist of the fibre. It might pollutes the surface and light is scattered out. Also it is thinkable that CsOH (from a caesium reaction with water) etches the silica [22] and constrains the transmission properties of the fibre.

5.3.3 Cleaning the fibre with light

As mentioned above, the transmission trough the OMF decreases when exposed to caesium vapour for over two weeks. If this is due to caesium sticking on the waist of the OMF, it might be possible to remove it (partially).

For this, light of higher power ($1 \mu\text{W}$ to $250 \mu\text{W}$) is coupled into the OMF by changing the neutral density filters in the setup (see Fig. 5.1). Fig. 5.6

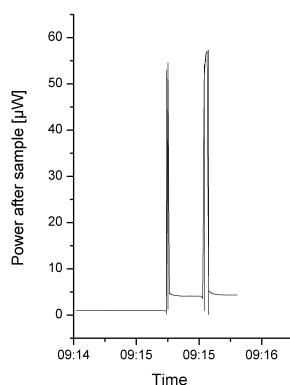


Figure 5.6: Increasing transmission by “shots”.

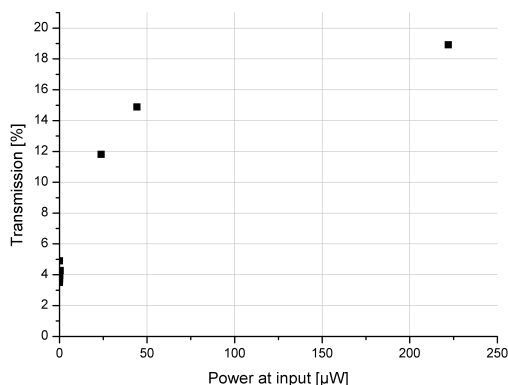


Figure 5.7: The transmission through the OMF depends on the input power.

shows the output power of the sample while removing all the filters for a short time (shot). After reinstalling the filters, the transmitted power is higher than before. The fibre waist has been cleaned.

Comparing the transmission through the OMF for different powers results in Fig. 5.7. For powers higher than 200 μW the transmission has reached its original value of 20%. After “cleaning” the fibre with light and reducing the power back to a very low value (required for the absorption measurement), the transmission still is much lower. This is not due to a new contamination with caesium atoms since this effect was also measurable when the caesium has been removed from the chamber.

It can be the case that not all of the caesium sticking to the fibre was removed. Even though there was no gaseous caesium detectable any more with the spectroscopy method, it could still stick to the waist and scatter out a constant, small proportion of the light. This of course affects rather low power beams. Unfortunately the caesium detection measurements are exactly done with lower powers. Hence, a “spoiled” OMF has to be replaced.

Chapter 6

Third harmonic generation with caesium

When a caesium vapour around the OMF has been obtained and detected, the high intensities in the evanescent field of the fibre can be used to generate third harmonic light from the caesium atoms. The strength of the generated light in the presence and absence of caesium is compared in this chapter.

6.1 Setup

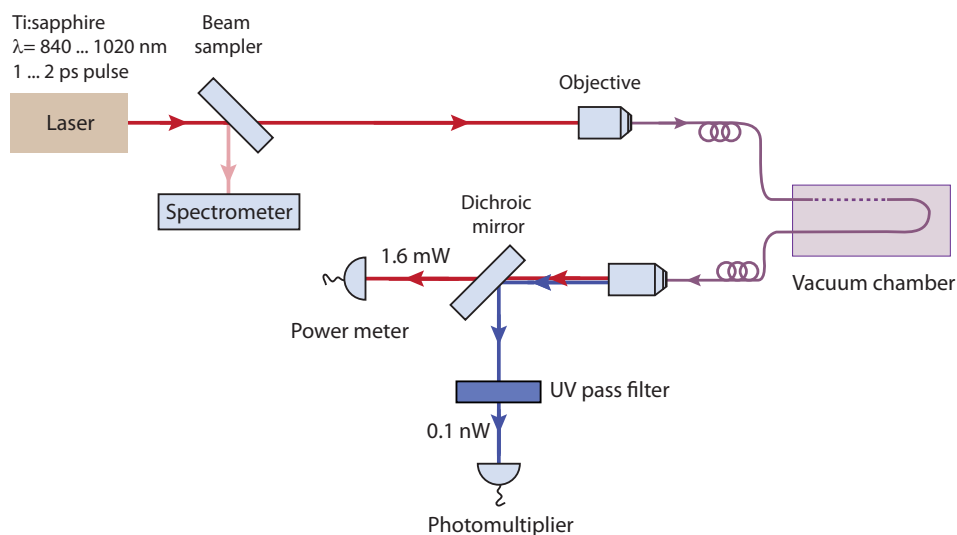


Figure 6.1: Setup used to detect THG with an OMF.

The third harmonic light can be detected after the OMF using the setup shown in Fig. 6.1. To obtain the needed high powers in the OMF (see section 3.1), a Ti:sapphire laser is used in pulsed mode ($\lambda = 840 - 1020$ nm,

pulse length $\sim 1 - 2$ ps) and coupled into the OMF. The wavelength of the laser has to be tuned to a wavelength, where the phase matching condition (depending on the waist diameter of the OMF) is fulfilled (see section 2.3.3). Third harmonic light in the UV range then is generated: by the fused silica of the fibre, as well as by the caesium atoms around the waist.

The generated third harmonic light is very weak (~ 0.1 nW) compared to the power of the Ti:Sapphire laser after the OMF (1.6 mW in the infrared). Hence, the UV light has to be detected with a photomultiplier (PMT). Even though the PMT is blind for infrared light, filtering it is necessary to avoid heating of the PMT which can cause charge movement and increase the noise. To separate the UV from the infrared light after the output of the OMF, a dichroic mirror is used. It transmits infrared light and reflects the UV third harmonic light. Still a small amount of infrared light can be reflected by this mirror (0.01 %), this is why an additional UV-pass filter is installed right before the PMT. That way, it is possible to detect the third harmonic light with low noise which will be tested as a next step.

6.2 Characterising THG without caesium

THG is measured with the above mentioned setup. The measurement is done without caesium fist, using the non-zero $\chi^{(3)}$ of silica to generate third harmonic light. This is to have a comparison value and to study the behaviour of the THG in the chamber. For the measurement, the infrared power after the OMF is kept constant at 1.6 mW at 944 nm (phase matching condition for the used fibre sample). Also the pulse width is not changed in order to be able to compare the results.

Since the chamber is flushed with dry nitrogen while a sample is installed, the taken reference value is for a nitrogen atmosphere. The THG is also monitored while pumping the nitrogen out of the chamber. It turns out that the pumping process has a big influence on the THG. Its strength can change by more than 50 %. Hence, a more detailed investigation of the influence of nitrogen (and air) on the THG can be found in the appendix (section A).

A comparison of the strength of the THG in nitrogen, in vacuum and in baked vacuum (30 hour at 80 °C) for the same OMF is summarised in table 6.1. The THG in vacuum is over three times higher than in dry nitrogen. After baking at 80 °C, the THG is approximately 20 % lower than before baking, but still higher than in nitrogen. This could indicate the influence of water on the THG (see section A).

Even though the reference values for the THG are fluctuating, an improvement with caesium should still be visible due to its higher $\chi^{(3)}$.

| PMT signal, V | | | |
|---------------|-----------|--------------|------------|
| In nitrogen | In vacuum | After baking | In caesium |
| 2.4(5) | 7.8(5) | 6.3(5) | 1.2(5) |

Table 6.1: Third harmonic strength in different atmospheres, measured with a PMT gain of 1.5×10^6 and an infrared power of 1.6 mW at 944 nm.

6.3 THG in caesium vapour

The reference values of the THG in nitrogen and in vacuum are now compared with caesium. The same setup as shown in Fig. 6.1 is used.

The caesium valve is opened and kept open for 10 days, such that the vapour pressure of caesium is already high but not too high to affect the transmission properties of the OMF (compare section 5.3.2). The presence of caesium is checked with the spectroscopy setup (section 5.1.3).

Once the presence of caesium is confirmed, third harmonic light is generated. The infrared power is kept at 1.6 mW again. The UV light should be generated by both, silica and caesium. The result of this measurement is shown in table 6.1. The strength of the THG in caesium is lower than without caesium (6.5 times lower than in vacuum).

After measuring for less than two minutes and shining in 1.6 mW during this time, the transmission started dropping. This transmission drop during measuring with higher powers (in the milliwatt range) has been observed several times. However, the measurements done in section 5.3.2 did not show such an early “pollution” of the fibre after 10 days. It could therefore be a light induced effect. In vacuum the fibre is not cooled by air. Hence, the high light power heats up the fibre waist. This energy might start a chemical reaction with caesium. The fibre could not be “cleaned with light” (section 5.3.3) afterwards.

6.4 Discussion

It has been observed that the strength of the THG varies a lot in different atmospheres (table 6.1). The enhanced THG due to caesium could not be observed. Still it remains unclear whether the measured third harmonic light is only due to silica, or also generated by caesium.

I have contacted Prof. Jim Franson from the University of Maryland who has done experiments with rubidium vapour around OMF [26]. He has observed a similar drop in the fibre transmission if the fibre is exposed to the atoms for too long. He suggests that the rubidium can form clusters on the fibre waist and these clusters can scatter light.

The same could be true for caesium. Clusters on the fibre would affect UV light more than infrared light. Therefore the loss of UV light would

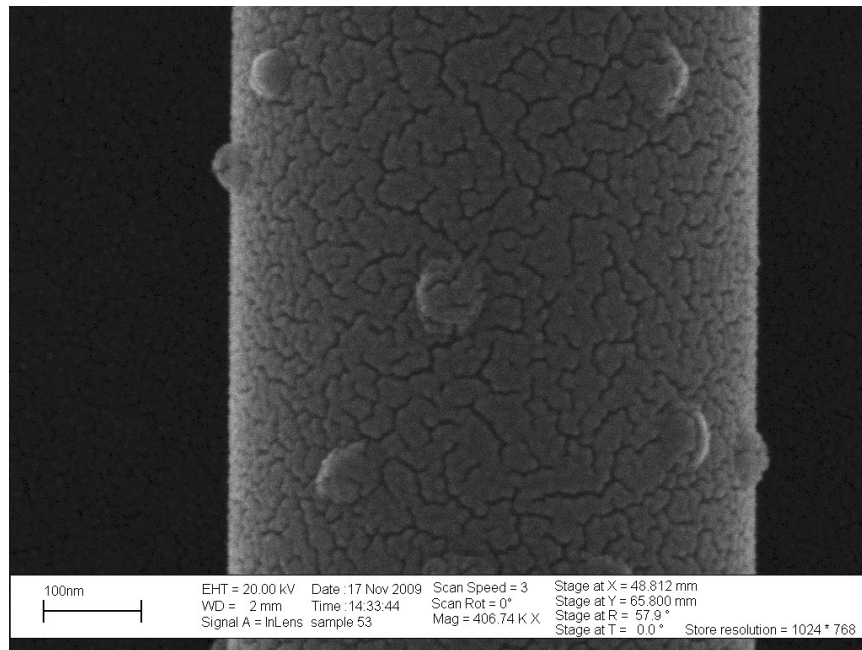


Figure 6.2: SEM picture of a gold coated OMF waist. The visible bumps are due to high UV powers [27].

be larger than the drop in infrared transmission, which is what I observed: increasing the infrared power back to 1.6 mW to even out the lower transmission, did not make the third harmonic recover to its initial value.

Also the caesium could react with the silica, as seen in the mentioned light induced effect. Residual water can react with caesium to form CsOH which is known to etch glass [22]. This also matches the observation in appendix A which indicates the influence of water on the THG. Both effects, the etching and the clustering, destroy the uniformity of the waist. The diameter of the waist would no longer stay constant which results in a worsened THG.

It is known from measurements with an electron microscope that UV light can produce bumps on the fibre surface [27] (Fig. 6.2). The mentioned unevenness of the waist hence can also be produced due to a high amount of UV light. It is imaginable that a lot of third harmonic light has been produced by the caesium and corrupted the the waist of the OMF.

Unfortunately the limited time of this work did not allow more measurements to study these problems.

Chapter 7

Summary and outlook

It has been shown in this work that an optical microfiber can be fed into a vacuum-tight chamber where harmonic light could be generated under controlled atmospheres. It has been found that the surrounding atmosphere has a significant influence on the harmonic generation, which might be explained by the amount of water present in the chamber.

Also it was possible to prepare a caesium vapour atmosphere around the optical microfiber where already small amounts of caesium atoms could be detected reliably. This demonstrates that microfibres are a useful and sensitive tool for spectroscopy.

Third harmonic light also could be obtained in a caesium vapour around the optical microfiber. However, the caesium vapour did not enhance THG as expected due to its high nonlinearity. It remains unclear whether significant third harmonic light was generated by the caesium in addition to the THG from the OMF itself. During my work there was only time for one trial with a fibre of suboptimal diameter. Therefore the measurement with caesium should first of all be repeated. Optimally one should produce a fibre that generates third harmonic light closer to the resonances of caesium. This could improve the $\chi^{(3)}$ by a factor of 10. For this purpose the fibre pulling process has to be improved to obtain a higher precision in the waist diameter.

Since the transmission properties of the fibre also have decreased during the measurement, it seems plausible that caesium has formed clusters on the waist of the OMF. UV light could thus be scattered out if still generated. The presence of such clusters should be checked with an electron microscope to further investigate this problem. If present, one could prevent clusters by adding an extra heating wire above the fibre waist. This wire should have a higher temperature than the chamber and should reduce the amount of caesium condensing on, or sticking to the fibre.

The electron microscope also would answer the question, whether a too high intensity of UV light has damaged the fibre by forming microscopic

bumps on the fibre waist. Such damage has been observed by D. Pritzkau [27] already. Yet the origin of these bumps has remained unclear so far.

Another idea for THG is the usage of different materials with high $\chi^{(3)}$ which are easier to handle. An example would be a nonlinear molecule that could be adsorbed on the fibre.

Appendices

Appendix A

Harmonic generation without caesium

During preparing the measurement for THG with caesium (6.2), it has been observed that pumping out nitrogen of the vacuum chamber has an effect on the THG. This behaviour has been studied for different atmospheres.

A.1 Third harmonic generation in air and vacuum

THG is measured with the same setup as used before for THG with caesium (Fig. 6.1). The power of the third harmonic light is monitored during pumping out air of the vacuum chamber. The infrared power after the sample and the laser pulse length are kept constant during the measurement.

The behaviour of the measured third harmonic power during pumping out is shown in Fig. A.1 (measured with 5 mW of infrared light and a PMT gain of 2×10^5): The third harmonic power drops immediately after the turbomolecular pump is switched on (pressure in the chamber $\sim 10 \times 10^{-3}$ mbar) while the infrared power stays constant. Ventilating the chamber with air, makes the third harmonic almost recover completely.

When the pump is started, a strong fluctuation in the THG power is visible for a short time. The same is true for the purging process when the ventilation valve is opened. This could be a vibration effect of the fibre due to the change in pressure.

A.2 THG in vacuum and dry nitrogen

To better understand why pumping out air causes a drop of the THG, the experiment is repeated with dry nitrogen and another OMF. The power and the PMT gain are kept at the same values (5 mW of infrared light, PMT gain 2×10^5). However the THG strength can not be directly compared to

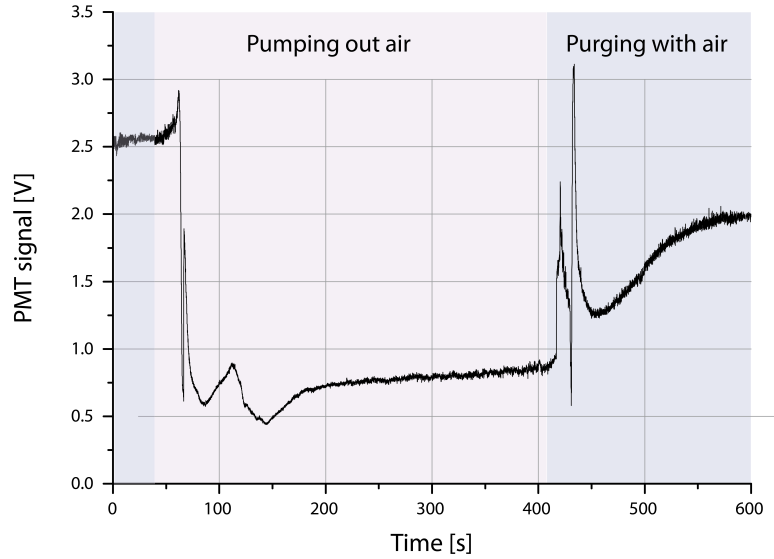


Figure A.1: THG during pumping out and ventilating with air

the previous measurement since it is a different OMF (with a different waist length).

Pumping out the air of the vacuum chamber (Fig. A.2) again shows the same behaviour as observed in the previous measurement: the third harmonic power drops in vacuum. But when the chamber is purged with dry nitrogen, the third harmonic power does not increase back to its initial value. It even is a little bit lower than before. By pumping out the nitrogen again, the third harmonic power can be increased back to a value close to the initial vacuum value. Purging the vacuum with air lets the third harmonic power recover to a value close to before the experiment.

During the measurements, the infrared power after the OMF was not influenced by the different atmospheres and stayed constant.

A.3 SHG in air, vacuum and dry nitrogen

To further investigate the sensitivity of the THG to the surrounding atmosphere, it is investigate whether this effect is restricted to the THG only. Hence, the second harmonic generation from the fibre has been studied. Second harmonic light is generated in the OMF by a surface effect despite the centrosymmetric lattice of the fibre(2.3.2).

The setup to detect SHG is the same as used for third harmonic detection (Fig. A.3) with the exception of the dichroic mirror and the UV-pass filter. Since the second harmonic light is generated in the visible wavelength range, the mirror is replace by a cold mirror (Thorlabs FM03), which reflects visible

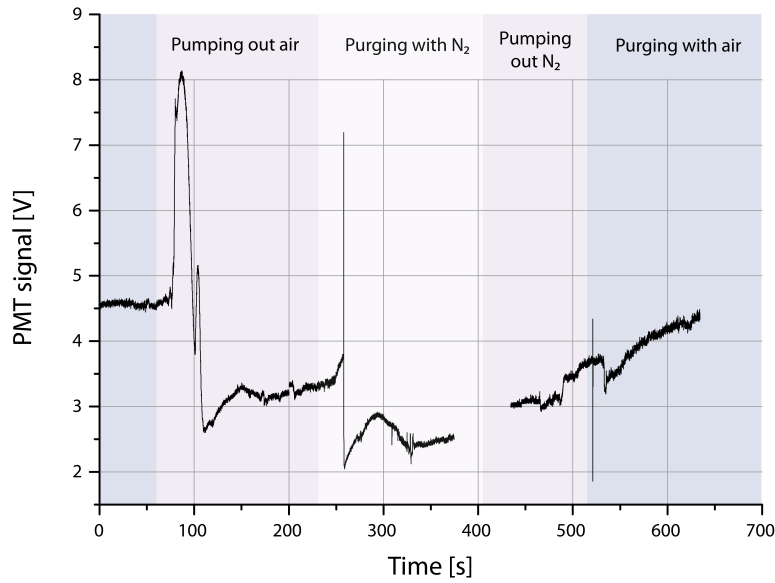


Figure A.2: THG during pumping out and ventilating with dry nitrogen

light and transmits infrared. The filter is exchanged with a VIS-pass filter.

SHG has been measured during pumping out the chamber and purging it with room air and dry nitrogen respectively. The result is comparable to the behaviour of the THG: the power of the second harmonic light drops during pumping out air but increases back when ventilating with air. In nitrogen the second harmonic remains at a value similar to the one in vacuum or lower.

During all the measurements, the infrared power again was constant at 5 mW. The experiment has been repeated with several different fibres. The strength of the drop in the second harmonic power during pumping out air does not seem to be related to specific OMF parameters (like the waist length or the slope of the taper).

Only one OMF exhibited a different behaviour than described above. The second harmonic light generated in that fibre was not affected by the pumping and ventilating process at all. The wavelength of this light was 500 nm, whereas the other examined samples generated second harmonic light between 420 nm to 480 nm due to their thinner waist diameter (see section 2.3.3). This indicates the wavelengths dependence of the measured effects.

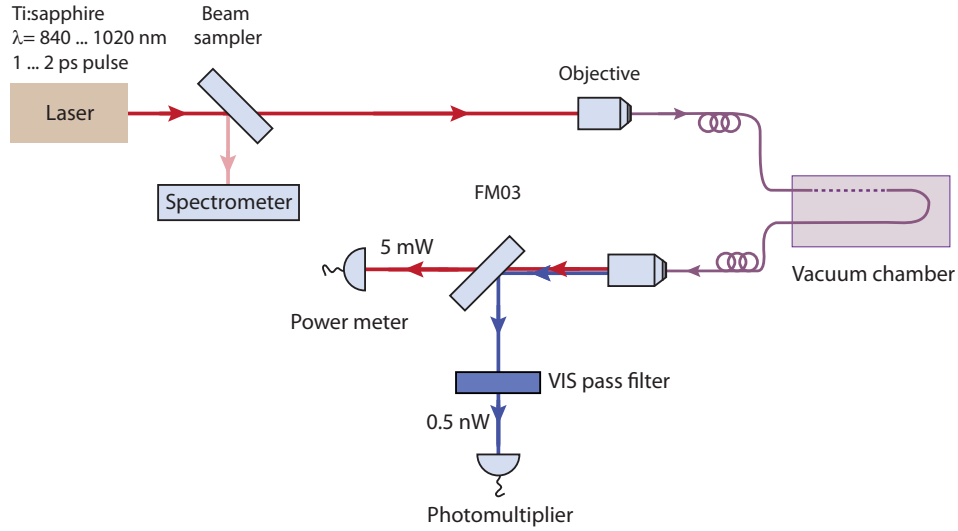


Figure A.3: Setup used to detect SHG with a OMF.

A.4 OMF transmission in air and vacuum

It is unknown whether the drop of the harmonic generation during pumping out the chamber has something to do with the light generation process itself, or with the transmission properties of the fibre. To study whether this effect is a wavelength dependent transmission effect, a blue laser with a wavelength of 405 nm is coupled into that very OMF that generated second harmonic light at 500 nm which was not affected by the pumping process (see section A.3).

The laser light with a power of 70 μW is coupled into the OMF and the transmitted power is directly measured with a power meter. During pumping out air, a drop of 20 % in the transmitted power is observed (Fig. A.4). During ventilating with air, the transmission recovers. Even though the drop in transmission is smaller than observed for THG and SHG, there is a clear effect on the transmission visible when opening the valves.

The same measurement is repeated with a battery-driven green laser pointer at 532 nm with 65 μW . During pumping out and ventilating with air, the transmission of the green light did not show a clear drop or increase (Fig. A.4). The constant decrease in the transmitted power is due to the battery of the laser.

Since a clear dependence of the transmission on the wavelength has been detected, it is interesting to know which wavelengths exactly are influenced in its transmission during pumping out the chamber. For this purpose a white light source is coupled to the OMF. The transmission through the sample is monitored with a spectrometer. The spectrum before and after pumping out the chamber are compared but no change is visible. This might

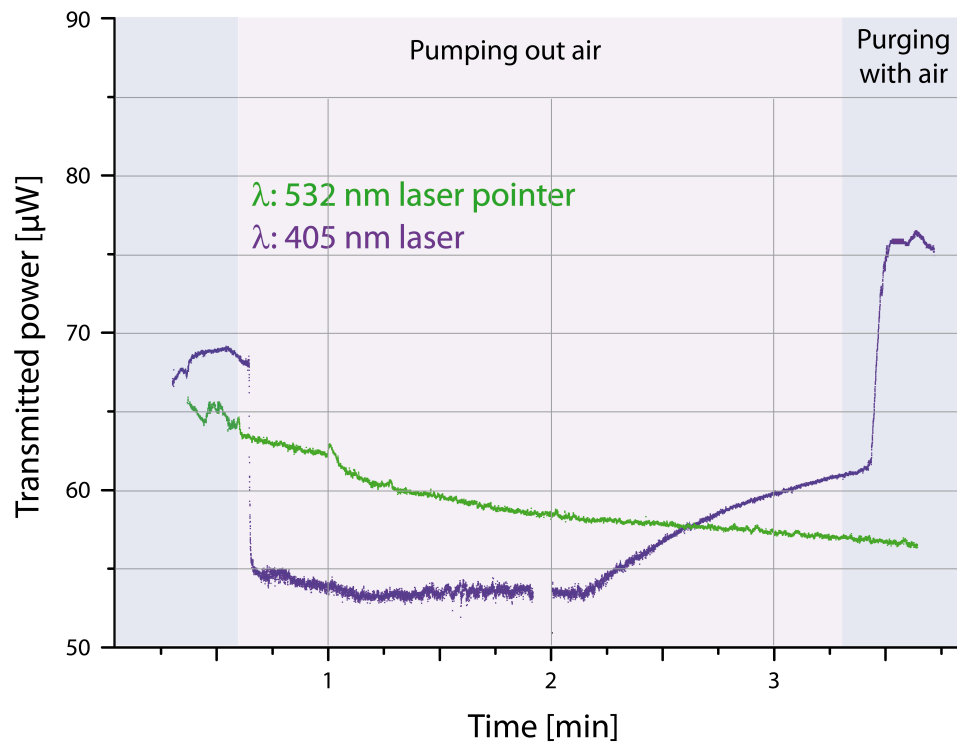


Figure A.4: Transmission of blue and green laser light through the OMF during pumping out and ventilating with air.

be due to the low powers of the white light source in that wavelength range.

A.5 Results and discussion

It has been observed that the atmosphere surrounding an OMF has an influence of the harmonic generation and on the transmission properties of the fibre at certain wavelengths.

The power of the third- and second-harmonic light (wavelengths between 280 nm to 480 nm) is effected in the following way:

$$P_{\text{nitrogen}} \leq P_{\text{vacuum}} < P_{\text{air}}$$

where P is the power of the third or second harmonic light, measured after the OMF.

An explanation for the degree of the drop during pumping out is not obvious to me. However, a dependence on the wavelength of the light could be observed. Light above 500 nm seems to be not influenced by the surrounding atmosphere. This is not only true for the harmonic generation, but also for the pure transmission property of the fibre: the transmission of light with wavelengths shorter than 500 nm was influenced by the atmosphere surrounding the OMF.

Hence, it is difficult to determine the origin of the influence on the harmonic light. One could reason that the drop in transmission affects the harmonic generation non-linearly. Still the reason for this drop remains unclear. The harmonic generation itself could be influenced by water. As shown by S. Zobotnov, water in porous silica increases its $\chi^{(3)}$ compared to porous silica filled with air [28]. Also Chun-An Tsai was able to enhance SHG in fused silica with water [29]. He claims that water can form dipole moments on the surface of the silica.

This is a reasonable explanation for the behaviour that I have measured. In air, the amount of water is high due to humidity. In dry nitrogen, on the other hand, the amount of water is very low. However in vacuum the amount of water is clearly lower than in air but there can be outgassing from the walls of the chamber. Since during this measurement the chamber was not baked out, this matches the observed behaviour.

To confirm that there is an influence of water, the measurement could be repeated in a wet nitrogen atmosphere. During this work unfortunately there was no time to do this any more. I concentrated on the final goal to obtain a caesium vapour around the fibre.

Bibliography

- [1] Gilberto Brambilla, Vittoria Finazzi, and David Richardson. “Ultra-low-loss optical fiber nanotapers”. In: *Opt. Express* 12.10 (2004), pp. 2258–2263.
- [2] Florian Warken, Arno Rauschenbeutel, and Thomas Bartholomäus. “Fiber Pulling Profits from Precise Positioning”. In: *Photonics Spectra* 42.3 (Mar. 2008), p. 73.
- [3] Florian Warken and Harald Giessen. “Fast profile measurement of micrometer-sized tapered fibers with better than 50-nm accuracy”. In: *Opt. Lett.* 29.15 (2004), pp. 1727–1729.
- [4] Limin Tong, Jingyi Lou, and Eric Mazur. “Single-mode guiding properties of subwavelength-diameter silica and silicon wire waveguides”. In: *Opt. Express* 12.6 (2004), pp. 1025–1035.
- [5] Allan Snyder and John Love. *Optical waveguide theory*. London: Chapman & Hall, 1983.
- [6] Konstantin Karapetyan. “Optical Fibre Toolbox”. In: <http://www.mathworks.com/matlabcentral/fileexchange/27819-optical-fibre-toolbox> (2010).
- [7] Govind Agrawal. *Nonlinear Fiber Optics*. 3rd. Optics and Photonics. Academic Press, 2001, p. 467.
- [8] D. A. Akimov et al. “Generation of a spectrally asymmetric third harmonic with unamplified 30-fs Cr:forsterite laser pulses in a tapered fiber”. In: *Appl. Phys. B* 76 (2003), pp. 515–519.
- [9] Victor Grubsky and Arthur Savchenko. “Glass micro-fibers for efficient third harmonic generation”. In: *Opt. Express* 13.18 (2005), pp. 6798–6806.
- [10] U. Österberg and W. Margulis. “Experimental studies on efficient frequency doubling in glass optical fibers”. In: *Opt. Lett.* 12.1 (1987), pp. 57–59.
- [11] Victor Grubsky and Jack Feinberg. “Phase-matched third-harmonic UV generation using low-order modes in a glass micro-fiber”. In: *Opt. Commun.* 274.2 (2007), pp. 447–450.

- [12] Jesper Lægsgaard. “Theory of surface second-harmonic generation in silica nanowires”. In: *J. Opt. Soc. Am. B* 27.7 (2010), pp. 1317–1324.
- [13] Ulrich Wiedemann et al. “Measurement of submicrometre diameters of tapered optical fibres using harmonic generation”. In: *Opt. Express* 18.8 (2010), pp. 7693–7704.
- [14] A. T. Georges, P. Lambropoulos, and J. H. Marburger. “Two-photon-resonant third-harmonic generation in cesium vapor”. In: *Optics Communications* 18.4 (1976), pp. 509–512.
- [15] R B Miles and S E Harris. “Optical Third-Harmonic Generation in Alkali Metal Vapors”. In: *IEEE Journal of Quantum Electronics* (1973).
- [16] C B Alcock. “Vapor Pressure Equations for the Metallic Elements 298 - 2500 K”. In: *Canadian Metallurgical Quarterly* (1984).
- [17] Daniel Adam Steck. *Cesium D Line Data*. Tech. rep. University of Oregon, 1996.
- [18] M. Thalhammer and A. Penzkofer. “Measurement of Third-Order Nonlinear Susceptibilities by Non-Phased Matched Third-Harmonic Generation”. In: *Appl. Phys. B* (1983).
- [19] U. Gubler and C. Bosshard. “Optical third-harmonic generation of fused silica in gas atmosphere: Absolute value of the third-order nonlinear optical susceptibility”. In: *Phys. Rev. B* (2000).
- [20] *Laserspektroskopie*. Springer-Verlage, 1991.
- [21] Eric R.I. Abraham and Eric A. Cornell. “Teflon Feedthrough for Coupling Optical Fibers Into Ultrahigh Vacuum Systems”. In: *Appl. Opt.* 37.10 (1998), pp. 1762–1763.
- [22] F A Chambers and L S Wilkiel. “Cesium hydroxide etching of silicon”. In: *J. Micromech. Microeng.* (1993).
- [23] M Matsui and K Komurasaki. “Influence of laser intensity on absorption line broadening in laser absorption spectroscopy”. In: *Appl. Physics* (2006).
- [24] K P Nayak and K Hakuta. “Optical nanofiber as an efficient tool for manipulating and probing atomic fluorescence”. In: *Opt. Express* (2007).
- [25] G Sagu et al. “Cold-Atom Physics Using Ultrathin Optical Fibres: Light-Induced Dipole Forces and Surface Interactions”. In: *PRL* (2007).
- [26] S. M. Hendrickson, T. B. Pittman, and J. D. Franson. “Nonlinear transmission through a tapered fiber in rubidium vapor”. In: *J. Opt. Soc. Am. B* 26.2 (2009), pp. 267–271.

- [27] D Pritzkau. “Measurement of submicrometer diameters of tapered optical fibres using scanning electron microscopy”. MA thesis. Universität Bonn, 2010.
- [28] S Konorov-T Veselova I Smironova P Kashkarov S Zaboltnov A Fedotov and A Zheltikov. “Effective-medium-controlled third-harmonic generation in lamellar-nonuniform porous glass”. In: *Optics Communications* (2004).
- [29] V Chao-Wei-Kuo T Cheng W Liou C Tsai J Wang and A Wu. “Enhancement of SHG in fused SiO₂ by corona poling under water, water vapor and salty environments”. In: *J. of Marine Science and Technology* (2008).

Danksagung

Mein Dank gilt allen, die mich beim Erstellen dieser Arbeit unterstützt haben.

Zuallererst möchte ich mich bei Herrn Professor Meschede dafür bedanken, dass ich meine Diplomarbeit an diesem lehrreichen Experiment erstellen durfte. Mein weiterer Dank gilt Professor Fiebig für die Übernahme des Korreferats.

Ein besonderes Danke möchte ich an meinen Betreuer Konstantin Karapetyan, Ulrich Wiedemann, Cristian Dan und auch Wolfgang Alt richten. Sie hatten während der gesamten Zeit ein offenes Ohr für mich und waren geduldige und hilfsbereite Ansprechpartner.

Allen weiteren Mitgliedern der Arbeitsgruppe und des Instituts danke ich für die entspannte Forschungs-Atmosphäre, die mich die Wahl dieses Instituts zur Erstellung einer Diplomarbeit niemals hat bereuen lassen.

Erklärung

Ich versichere, dass ich diese Arbeit selbständig verfasst und keine anderen als die angegebenen Quellen und Hilfsmittel benutzt, sowie die Zitate kenntlich gemacht habe.

Referent: Prof. Dr. D. Meschede
Korreferent: Prof. Dr. M. Fiebig